HHS Public Access

Author manuscript

Oncogene. Author manuscript; available in PMC 2018 September 22.

Published in final edited form as:

Oncogene. 2018 June ; 37(26): 3528–3548. doi:10.1038/s41388-018-0190-7.

A RAS-CaMKKβ-AMPKα2 pathway promotes senescence by licensing post-translational activation of C/EBPβ through a novel 3′UTR mechanism

Sandip K. Basu[1,6], **Mesfin Gonit**[1,6], **Jacqueline Salotti**[1], **Jiji Chen**[2], **Atharva Bhat**[2], **Myriam Gorospe**[3], **Benoit Viollet**[4], **Kevin P. Claffey**[5], and **Peter F. Johnson**[1,7]

[1]Mouse Cancer Genetics Program, Center for Cancer Research, National Cancer Institute, Frederick, MD, USA

[2]Leidos Biomedical Research, Inc., Frederick National Laboratory for Cancer Research, Frederick, MD, USA

[3]Laboratory of Genetics, National Institute on Aging-Intramural Research Program, National Institutes of Health, Baltimore, MD, USA

[4]INSERM, U1016, Institut Cochin, 75014 Paris, France; CNRS, UMR8104, 75014 Paris, France; Université Paris Descartes, Sorbonne Paris Cité, 75014 Paris, France

[5]Department of Cell Biology, University of Connecticut Health Center, Farmington, CT, USA

Abstract

Oncogene-induced senescence (OIS) is an intrinsic tumor suppression mechanism that requires the p53 and RB pathways and post-translational activation of C/EBPβ through the RAS-ERK cascade. We previously reported that in transformed/proliferating cells, C/EBPβ activation is inhibited by G/U-rich elements (GREs) in its 3′UTR. This mechanism, termed "3′UTR regulation of protein activity" (UPA), maintains C/EBPβ in a low-activity state in tumor cells and thus facilitates senescence bypass. Here we show that C/EBPβ UPA is overridden by AMPK signaling. AMPK activators decrease cytoplasmic levels of the GRE binding protein HuR, which is a key UPA component. Reduced cytoplasmic HuR disrupts 3′UTR-mediated trafficking of *Cebpb* transcripts to the peripheral cytoplasm – a fundamental feature of UPA – thereby stimulating C/EBPβ activation and growth arrest. In primary cells, oncogenic RAS triggers a Ca^{++}-CaMKKβ-AMPKα2-HuR pathway, independent of AMPKα1, that is essential for C/EBPβ activation and OIS. This axis is disrupted in cancer cells through down-regulation of AMPKα2 and CaMKKβ. Thus, CaMKKβ-AMPKα2 signaling constitutes a key tumor suppressor pathway that activates a

[7]Correspondence should be addressed to P.F.J. (johnsope@mail.nih.gov).
[6]These authors contributed equally to this work.

Present addresses

Mesfin Gonit: Lentigen Tech, Inc., Gaithersburg, MD, USA
Jiji Chen: Advanced Imaging and Microscopy Resource, National Institutes of Health, Bethesda, MD, USA

CONFLICT OF INTEREST

The authors declare no conflict of interest.

novel UPA-cancelling mechanism to unmask the cytostatic and pro-senescence functions of C/EBPβ.

Keywords

oncogene-induced senescence; oncogenic RAS; C/EBPβ; AMPK; 3′UTR

INTRODUCTION

Cellular stresses such as metabolic imbalances, DNA damage, or activated oncogenes can induce senescence, a stable form of growth arrest that plays a key role in eliminating damaged cells and suppressing cancer[1,2]. Senescent cells frequently express a panel of pro-inflammatory cytokines and growth factors, their receptors, and matrix proteases collectively known as the "senescence-associated secretory phenotype" or SASP[3]. C/EBPβ, along with the tumor suppressors p53 and Rb, is required for oncogene-induced senescence (OIS) in primary fibroblasts. C/EBPβ is an auto-inhibited protein that becomes post-translationally activated by oncogenic RAS signaling via the RAF-MEK-ERK cascade, which induces phosphorylation on several C/EBPβ residues that stimulate its DNA-binding, homodimerization, and transactivation functions[4,5]. The de-repressed form of C/EBPβ has cytostatic activity and cooperates with NF-κB to regulate numerous SASP genes in senescent cells[6–9].

Interestingly, C/EBPβ activity is suppressed in immortalized and transformed cells, but not in senescent primary cells, by the 3′ untranslated region (3′UTR) of its mRNA[10]. This novel mechanism, termed "3′UTR regulation of protein activity" (UPA), requires a 100 nt 3′UTR sequence encompassing several G/U-rich elements (GREs). The GRE inhibits C/EBPβ activity by localizing *Cebpb* transcripts to a peripheral region of the cytoplasm. In this location, newly-translated C/EBPβ is inaccessible to its activating kinase, p-ERK1/2, which is confined to a separate perinuclear cytoplasmic domain in cells expressing oncogenic RAS (Fig. 1a)[10]. By preventing C/EBPβ phosphorylation/activation, UPA contributes to senescence bypass in cancer cells. C/EBPβ UPA also requires the ARE/GRE binding protein, HuR (ELAVL1), which associates with the *Cebpb* GRE region. HuR is a ubiquitously-expressed factor that controls the stability or translation of many mRNAs and shuttles between the cytoplasm and nucleus in a regulated manner that governs its cytoplasmic availability[11,12]. Elevated cytoplasmic HuR is frequently observed in tumors and correlates with increased malignancy and poor prognosis[13,14], consistent with HuR's role in repressing the cytostatic activity of C/EBPβ[10] as well as stabilizing mRNAs that encode mitogenic proteins such as cyclins[15].

AMP-activated kinase (AMPK) is a key cellular energy sensor whose activity is stimulated by elevated AMP/ATP ratios in response to metabolic stresses such as glucose deprivation, mitochondrial dysfunction, and hypoxia[16]. Activated AMPK promotes metabolic reprogramming by phosphorylating proteins that restore energy homeostasis[16,17], but can also elicit cell cycle arrest, in part by inducing p53 and inhibiting mTOR signaling[17]. Accordingly, AMPK has anti-oncogenic functions[18] that may also involve its upstream

kinase, LKB1, a tumor suppressor that is lost in many cancers[19]. Since pharmacological AMPK activators such as metformin are under evaluation for cancer treatment and prevention, it is important to elucidate the effector pathways that mediate the anti-tumor effects of AMPK signaling.

AMPK has been linked to senescence of primary fibroblasts[20] by reducing cytoplasmic HuR levels[21,22]. This occurs through AMPK-mediated phosphorylation and subsequent acetylation of the nuclear transporter, importin α1, increasing its affinity for HuR and facilitating nuclear translocation[22]. Therefore, we hypothesized that AMPK signaling might disrupt C/EBPβ 3′UTR inhibition by reducing HuR availability, allowing conversion of C/EBPβ to its activated, pro-senescent form. Here we show that C/EBPβ is activated by AMPK agonists that override negative regulation by its 3′UTR, leading to a cytostatic response. Moreover, establishment of OIS in primary cells requires signaling through a RAS-CaMKKβ-AMPKα2-HuR pathway that negates C/EBPβ UPA. Our findings reveal a novel pro-senescence pathway triggered by oncogenic stress that is frequently disrupted in tumor cells.

RESULTS

AMPK signaling overrides *Cebpb* 3′UTR inhibition to stimulate C/EBPβ DNA-binding and cytostatic activity

To investigate whether AMPK signaling reverses C/EBPβ 3′UTR inhibition (UPA), we used 5-aminoimidazole-4-carboxamide ribonucleotide (AICAR) to activate AMPK in 293T cells transfected with C/EBPβ constructs lacking or containing the 3′UTR (*Cebpb*$^{\Delta UTR}$ or *Cebpb*^{UTR}, respectively). C/EBPβ proteins were expressed without or with HRAS^{G12V} and lysates were analyzed for DNA binding by EMSA using a C/EBP site probe (Fig. 1b). As expected[10], the 3′UTR suppressed RAS-induced augmentation of C/EBPβ DNA binding (compare β^{UTR} and β$^{\Delta UTR}$; Fig. 1b). However, 3′UTR inhibition was abrogated in cells treated with AICAR, while β$^{\Delta UTR}$ DNA binding was largely unaffected by the drug. AICAR also stimulated AMPK phosphorylation (p-T172) and decreased the cytoplasmic levels of HuR[21] (Fig. 1b). In addition, HRAS^{G12V} enhanced β$^{\Delta UTR}$-mediated transactivation of a C/EBP-driven reporter (2xC/EBP-Luc), whereas the transcriptional activity of β^{UTR} was only weakly activated by RAS (Fig. 1c). The 3′UTR inhibitory effect was again abolished by AICAR. Similarly, co-expression of a constitutively active form of the AMPKα2 catalytic subunit (CA-AMPK) reversed 3′UTR-mediated repression of C/EBPβ in DNA-binding and transactivation assays (Supplementary Fig. 1a,b).

We further examined the ability of AMPK to override UPA in NIH3T3^{RAS} cells, which express low endogenous C/EBPβ levels due to its down-regulation by oncogenic RAS[23,24]. Analysis of 3T3^{RAS} cells stably expressing *Cebpb*$^{\Delta UTR}$ or *Cebpb*^{UTR} confirmed that the 3′UTR repressed C/EBPβ DNA binding, with no significant effect on protein levels (Fig. 1d, lanes 2 and 3). However, co-expression of CA-AMPK stimulated C/EBPβ binding activity in *Cebpb*^{UTR} cells, which was comparable to that of *Cebpb*$^{\Delta UTR}$ without CA-AMPK (compare lanes 2 and 6). Cell proliferation assays showed that the presence of activated C/EBPβ, either through expression of *Cebpb*$^{\Delta UTR}$ alone or *Cebpb*^{UTR} co-expressed with CA-AMPK, caused growth arrest (Fig. 1e) accompanied by an increase in senescent (SA-βGal^{+})

cells (Fig. 1f; Supplementary Fig. 1c). CA-AMPK alone did not appreciably inhibit proliferation or induce senescence in $3T3^{RAS}$ cells. Notably, CA-AMPK did not further enhance the cytostatic or DNA-binding functions of $Cebpb^{\Delta UTR}$, indicating that AMPK stimulates C/EBPβ activity predominantly by reversing 3′UTR inhibition. $3T3^{RAS}$-$Cebpb^{\Delta UTR}$ cells potently up-regulated SASP genes (*Il1a*, *Il6*, and *Cxcl1*) compared to $3T3^{RAS}$ cells, while this induction was not observed in $3T3^{RAS}$-$Cebpb^{UTR}$ cells (Supplementary Fig. 1d). Interestingly, CA-AMPK failed to activate SASP genes in $Cebpb^{UTR}$–expressing cells despite stimulating C/EBPβ DNA binding and, in fact, reduced expression of these genes in $Cebpb^{\Delta UTR}$ cells. CA-AMPK also inhibited RAS-induced activation of NF-κB (i.e., nuclear p65 levels; Supplementary Fig. 1e), supporting prior observations that AMPK can suppress inflammation by blocking NF-κB signaling[25–27]. Thus, NF-κB blockade by AMPK at least partly accounts for the failure to induce SASP genes.

To determine whether AMPK alters 3′UTR-dependent peripheral localization of *Cebpb* transcripts, we examined the cytoplasmic location of *Cebpb* mRNAs in NIH3T3 cells using the MS2-GFP-nls RNA tagging system[10,28]. Confocal microscopy revealed that 8xMs2b-tagged $Cebpb^{\Delta UTR}$ transcripts were distributed uniformly in the cytoplasm, whereas 8xMs2b-$Cebpb^{UTR}$ mRNAs were excluded from the perinuclear region and were more abundant in the cell periphery (Fig. 2a). However, co-expression of CA-AMPK disrupted the peripheral localization of $Cebpb^{UTR}$ transcripts, generating a pan-cytoplasmic pattern similar to that of $Cebpb^{\Delta UTR}$. CA-AMPK also caused nuclear translocation of HuR and increased phosphorylation of endogenous C/EBPβ on the Thr188 ERK site, as determined by IF imaging using a phospho-C/EBPβ antibody (Supplementary Fig. 1f), consistent with reversal of UPA inhibition.

We next used *in situ* hybridization (RNA FISH) to determine whether the location of endogenous *Cebpb* transcripts is affected by AMPK signaling. Appreciable cytoplasmic HuR was seen in control NIH3T3 cells, and *Cebpb* FISH signals were concentrated toward the cell periphery (Fig. 2b). However, AICAR treatment caused a strong reduction in cytoplasmic HuR, coinciding with more uniform *Cebpb* mRNA localization. To quantify these data in an unbiased manner, we developed an algorithm to assess *Cebpb* mRNA polarization. FISH signals were assigned to one of three cytoplasmic segments (inner, intermediate, outer), defined by boundaries placed at 1/3 and 2/3 of the radial distance between the nuclear and plasma membranes (Fig. 2c; see Methods). The distribution of mRNAs among the three segments was then determined. This method confirmed that AMPK activation decreased the proportion of *Cebpb* transcripts residing in the outer segment while increasing the nuclear-proximal fraction (Fig. 2d). Thus, AMPK signaling abrogates 3′UTR-mediated trafficking of *Cebpb* transcripts to the cell periphery, allowing RAS-induced post-translational activation of C/EBPβ translated from mRNAs located in the perinuclear region.

AMPK-induced cytostatic responses in tumor cells and primary MEFs involve activation of C/EBPβ

To extend our findings, we asked whether C/EBPβ activity is augmented by AMPK signaling in human cancer cells. CA-AMPK decreased the proliferation of A549 lung

adenocarcinoma cells, and this effect was partially reversed by C/EBPβ depletion (Fig. 3a). Similar results were observed in MCF7 breast cancer cells (Supplementary Fig. 2a). In addition, CA-AMPK modestly increased C/EBPβ DNA binding and enhanced homodimerization (homodimers are the cytostatic form of C/EBPβ)[9] (Fig. 3b). C/EBPβ was also activated by metformin, a commonly prescribed anti-diabetic that decreases cellular ATP levels by inhibiting complex I of the mitochondrial respiratory chain and thus indirectly activates AMPK[29], and by salicylate, recently shown to be a direct AMPK agonist[30]. Both agents stimulated AMPK phosphorylation (p-Thr172) and increased C/EBPβ DNA binding in A549 cells (Supplementary Fig. 2b). The increase in C/EBPβ DNA binding occurred despite a decrease in ERK1/2 activity (Supplementary Fig. 2b), consistent with studies showing that RAS-ERK signaling can be suppressed by AMPK activation[31]. The ability of salicylate to augment C/EBPβ DNA binding required AMPK, as this response was lost when both AMPKα isoforms (1 and 2) were simultaneously depleted (Supplementary Fig. 2c). Metformin and salicylate decreased cytoplasmic HuR levels and induced phosphorylation on C/EBPβ Thr235 (the ERK site in human C/EBPβ), while the increase in p-C/EBPβ was blocked by the MEK1/2 inhibitor, U0126 (Fig. 3c).

RNA FISH analysis showed that endogenous *CEBPB* transcripts are largely excluded from the perinuclear cytoplasm in A549 cells, while phospho-ERK1/2 is concentrated in this region (Fig. 3d). Both metformin and salicylate altered *CEBPB* mRNA polarization, increasing the proportion of transcripts located in the nuclear-proximal region. Quantitative analysis supported a statistically significant relocation of *CEBPB* mRNA to the juxtanuclear region upon AMPK activation (Fig. 3e), replicating the effect seen in NIH3T3 cells. Thus, in tumor cells AMPK agonists disrupt peripheral *CEBPB* mRNA localization and stimulate C/EBPβ activity, which partially mediates the cytostatic effects of these agents.

We next used an HuR mutant to confirm that HuR re-localization is critical for AMPK-induced activation of C/EBPβ. Phosphorylation on HuR Ser202 by Cdk1 stimulates nuclear translocation of HuR, and substitution of this residue with Ala (HuR^{S202A}) increases its cytoplasmic retention[32]. Although we found that stable expression of HuR^{S202A} is cytotoxic, it can be transiently expressed to test the role of HuR translocation in AMPK-induced activation of C/EBPβ. WT and mutant HuR proteins appended with a tandem affinity purification (TAP) tag were expressed in A549 cells and imaged using a TAP antibody. In unstimulated cells, both proteins showed comparable cytoplasmic abundance as well as a prominent nuclear pool (Supplementary Fig. 3a,b). However, salicylate significantly reduced the cytoplasmic levels of WT HuR, whereas HuR^{S202A} remained largely unaffected. Moreover, drug-treated cells expressing WT HuR showed increased phosphorylation on the C/EBPβ ERK site (Thr235 in human C/EBPβ), while HuR^{S202A} blocked this phosphorylation. HuR^{S202A} but not WT HuR also suppressed salicylate-induced activation of C/EBPβ DNA binding (Supplementary Fig. 3c). These data strongly support the notion that HuR eviction from the cytoplasm is a critical step in C/EBPβ activation by AMPK signaling.

We next addressed whether C/EBPβ is an effector of AMPK-induced growth arrest/senescence in primary cells. Expression of CA-AMPK inhibited proliferation of *WT* MEFs, whereas this response was significantly diminished in $Cebpb^{-/-}$ cells (Supplementary Fig.

4a). AMPK also enhanced C/EBPβ DNA binding in these cells and increased homodimer levels (Supplementary Fig. 4b). CA-AMPK expression coincided with elevated numbers of SA-β-Gal$^+$ cells in *WT* MEFs but not in *Cebpb*$^{-/-}$ MEFs (Supplementary Fig. 4c), and reduced cytoplasmic HuR levels in both *WT* and *Cebpb*$^{-/-}$ cells (Supplementary Fig. 4d). Similar results were obtained using salicylate to activate AMPK (Supplementary Fig. 5a–d). Conversely, treatment of MEFs with the AMPK inhibitor, compound C, increased cytoplasmic HuR levels and inhibited C/EBPβ DNA binding (Supplementary Fig. 5e).

AMPK signaling opposes cell proliferation in part by inhibiting mTORC1 activity[33,34]. To determine whether the cytostatic effects of AMPK involve activation of C/EBPβ downstream of mTORC1 blockade, we treated MEFs with the mTOR inhibitor, rapamycin. Rapamycin elicited similar cytostatic responses in *WT* and *Cebpb*$^{-/-}$ MEFs, showing that the anti-proliferative effect is independent of C/EBPβ (Supplementary Fig. 5f). Moreover, the drug failed to enhance C/EBPβ DNA binding despite inhibiting phosphorylation of the mTORC1 target, S6K (Supplementary Fig. 5g). Thus, AMPK signaling activates C/EBPβ and inhibits mTORC1 through independent pathways.

AMPKα2 is required for RAS-induced activation of C/EBPβ and OIS in MEFs

Our observation that C/EBPβ is an important effector of AMPK-driven senescence raised the possibility that AMPK-C/EBPβ signaling may also be involved in OIS. We initially sought to analyze MEFs lacking both AMPKα1 and 2 (DKO cells)[35], as these cells are devoid of all AMPK activity. However, low passage DKO cells proliferated very poorly, precluding their use in OIS studies (Supplementary Fig. 6a). MEFs lacking AMPKα1 alone also showed impaired growth in culture which was not further decreased by expression of HRAS^{G12V}, and these cells were highly senescent even in the absence of RAS (~60% SA-βGal$^+$) (Fig. 4a). By contrast, *Ampka2*$^{-/-}$ cells proliferated much more rapidly than *WT* MEFs and were largely refractory to RAS-induced growth arrest and senescence (Fig. 4b), consistent with previous observations[36]. Furthermore, C/EBPβ DNA binding was stimulated by HRAS^{G12V} in AMPKα1-depleted cells, like *WT* MEFs (Fig. 4c), but showed almost no induction in *Ampka2*$^{-/-}$ cells (Fig. 4d). Levels of activated ERK were similar in RAS-expressing *WT* and *Ampka2*$^{-/-}$ cells (Fig. 4d), indicating that lack of C/EBPβ activation is not due to reduced RAS-ERK signaling. Thus, AMPKα1 is dispensable for RAS-induced senescence and C/EBPβ activation despite being the major AMPKα subunit in MEFs[37], while the minor AMPKα2 isoform plays a critical role in OIS and C/EBPβ activation.

Since activated C/EBPβ promotes transcription of SASP genes, we asked whether their induction by HRAS^{G12V} is affected in *Ampka2*$^{-/-}$ cells. The six SASP genes tested were efficiently induced in *WT* MEFs; by contrast, three (*Il6*, *Cxcl1* and *Cxcl5*) showed severely diminished expression in AMPKα2 null cells (Fig. 4e). Levels of *Il1a* and *Ccr1* were increased in *Ampka2*$^{-/-}$ cells relative to *WT* MEFs, while *Cxcl2* was unaffected. Thus, AMPKα2 deficiency abrogates expression of a subset of SASP genes. As IL-6 has been shown to reinforce OIS through autocrine signaling[7], its impaired expression may contribute to the senescence bypass in *Ampka2*$^{-/-}$ MEFs. In MEFs depleted for AMPKα1, five of the SASP genes, except for *Ccr1*, showed moderately decreased expression (~50% of *WT*

levels) (Supplementary Fig. 6b). However, *Il6*, *Cxcl1* and *Cxcl5* levels were reduced to a much greater extent in cells lacking AMPKα2 than AMPKα1.

The residual level of C/EBPβ DNA binding in *Ampka2*$^{-/-}$ cells may be adequate to activate transcription of SASP genes such as *Il1a*, whose induction is also strongly dependent on NF-κB. To address the possible basis for increased *Il1a* expression in *Ampka2*$^{-/-}$ MEFs, we asked whether NF-κB activation was affected by loss of AMPKα2. IF assays of p65 subcellular distribution showed more efficient HRAS^{G12V}-induced nuclear translocation of p65 in *Ampka2*$^{-/-}$ cells than in *WT* MEFs (Supplementary Fig. 6c). Quantitative analysis confirmed that this difference was significant (Supplementary Fig. 6d). Thus, AMPKα2 may partially suppress NF-κB induction in senescent MEFs, although not sufficiently to block the SASP. Increased NF-κB activity may potentiate transcription of certain SASP genes such as *Il1a* in *Ampka2*$^{-/-}$ cells.

Oncogenic RAS and AMPK agonists act through different pathways to induce HuR translocation and C/EBPβ activation

We next investigated whether AMPKα2 regulates HuR nuclear translocation in senescing cells. Immunostaining revealed appreciable levels of cytoplasmic HuR in low passage *WT* MEFs, as expected for cells that retain the ability to proliferate (Fig. 5a). By contrast, expression of HRAS^{G12V} caused a marked decrease in cytoplasmic HuR, which was associated with enhanced phosphorylation on C/EBPβ Thr188. Comparable responses were seen in *Ampka1*$^{-/-}$ cells. In contrast, *Ampka2*$^{-/-}$ MEFs did not display RAS-induced HuR translocation or increased p-C/EBPβ levels (Fig. 5a,b; Supplementary Fig. 6e). Interestingly, the opposite results were observed in cells treated with AICAR. AICAR provoked nuclear translocation of HuR and C/EBPβ phosphorylation in *WT* and *Ampka2*$^{-/-}$ MEFs but not in *Ampka1*$^{-/-}$ cells. These data suggest that AMPKα2 mediates oncogenic RAS-induced HuR re-localization, C/EBPβ activation and senescence, whereas AMPKα1 is the critical sensor of metabolic stress and activates growth arrest/senescence pathways in response to increased AMP.

Since Importinα1 has been implicated in HuR nucleocytoplasmic shuttling[21,22], we examined its role in RAS-induced HuR translocation. In control MEFs, Impα1 displayed cytoplasmic staining along with a prominent ring at the nuclear envelope (Fig. 5c). Upon HRAS^{G12V} expression, Impα1 became primarily nuclear and the nuclear ring disappeared, coinciding with HuR nuclear uptake and increased C/EBPβ phosphorylation on Thr188. Depletion of Impα1 in RAS-expressing MEFs prevented HuR re-localization and blocked C/EBPβ phosphorylation. Moreover, RAS was unable to trigger Impα1 nuclear translocation in *Ampka2*$^{-/-}$ cells (Fig. 5d). Therefore, Impα1 is a critical component of the RAS-AMPKα2-HuR-C/EBPβ pathway that promotes cell cycle arrest and senescence.

The AMPK kinase CaMKKβ links oncogenic RAS to the AMPKα2-HuR-C/EBPβ pro-senescence pathway

We next sought to identify the upstream kinase that relays RAS signals to AMPKα2 to activate OIS. LKB1 is a known tumor suppressor and a major AMPK kinase[38,39]. We found that *Lkb1*$^{-/-}$ MEFs display normal RAS-induced growth arrest, as reported previously[40], as

well as activation of C/EBPβ DNA binding, Thr188 phosphorylation, and HuR re-localization (Fig. 6a; Supplementary Fig.7a,b). However, like *Ampka1*$^{-/-}$ cells, *Lkb1*$^{-/-}$ MEFs were refractory to AICAR-induced HuR nuclear translocation and C/EBPβ phosphorylation (Fig. 7a). Thus, LKB1 is dispensable for C/EBPβ activation and OIS, indicating that another AMPK kinase acts downstream of RAS. A possible candidate is CaMKKβ (CaMKK2), which can phosphorylate and activate AMPK in response to increased intracellular calcium[41,42]. Indeed, depletion of CaMKKβ in MEFs prevented RAS-induced HuR translocation and suppressed C/EBPβ phosphorylation (Fig. 6b,c). CaMKKβ-depleted cells also showed a substantial reversal of RAS-induced growth arrest and senescence (Fig. 6d,e). However, over-expression of CA-AMPKα2, which contains a phosphomimetic substitution at Thr172, restored growth arrest in CaMKKβ-depleted MEFs (Fig. 6d), suggesting that AMPKα2 is a key target of CaMKKβ in cells undergoing OIS. Treatment of cells with the CaMKK inhibitor, STO-609, also blocked RAS-induced C/EBPβ phosphorylation and senescence (Supplementary Fig. 7c,d). Since CaMKKβ is a Ca^{++}-dependent kinase, we examined the effects of a cell-permeant calcium chelator, BAPTA, on $HRAS^{G12V}$-induced responses. BAPTA treatment for 2 hr blocked HuR translocation and C/EBPβ phosphorylation in RAS-expressing MEFs (Fig. 6f). Collectively, these results demonstrate that $HRAS^{G12V}$-induced activation of the pro-senescence AMPKα2-HuR-C/EBPβ pathway requires CaMKKβ and mobilization of intracellular Ca^{++}.

Down-regulation of AMPKα2 and CaMKKβ is critical for oncogenic RAS-driven transformation and cancer

The essential role of the CaMKKβ-AMPKα2-HuR axis in RAS-induced senescence suggested that this pathway must be bypassed in tumor cells. Therefore, we analyzed the effect of oncogenic RAS on cytoplasmic HuR levels in MEFs and NIH3T3 cells to compare senescent and transformed fibroblasts, respectively. Immunoblotting confirmed that RAS decreased cytoplasmic HuR in MEFs (Fig. 7a), supporting the IF data. By contrast, cytoplasmic HuR was modestly increased in NIH3T3 cells, which was also seen by IF staining (Fig. 7b). However, $NIH3T3^{RAS}$ cells remained responsive to metformin-induced HuR nuclear translocation. Thus, RAS-induced HuR re-localization is abrogated in immortalized NIH3T3 cells. qRT-PCR analysis showed that *Ampka1* mRNA levels were unaffected by $HRAS^{G12V}$ in both MEFs and NIH3T3 cells and were comparable in all four cell populations (Fig. 7c). However, *Ampka2* transcripts were nearly 5-fold lower in control NIH3T3 cells compared to MEFs, and $HRAS^{G12V}$ further decreased them to nearly undetectable levels. Furthermore, CaMKKβ protein levels were decreased upon expression of $HRAS^{G12V}$ in NIH3T3 cells, but were modestly up-regulated by RAS in MEFs (Fig. 7d). Thus, low CaMKKβ and AMPKα2 levels in immortalized cells correlate with RAS-induced transformation and maintenance of cytoplasmic HuR.

To determine whether CaMKKβ and AMPKα2 down-regulation in $NIH3T3^{RAS}$ is causally related to bypass of RAS-induced senescence and instatement of C/EBPβ UPA, we expressed AMPKα2 ± CaMKKβ, without or with $Cebpb^{UTR}$. AMPKα2 alone reduced cell proliferation by ~30% (6-day time point), and $Cebpb^{UTR}$ decreased cell growth by a similar amount (Supplementary Fig. 8a). However, both proteins together reduced proliferation by nearly 75%, and a further decrease was observed when CaMKKβ was also co-expressed.

The two proteins also cooperated to induce senescence and increased expression of SASP genes (Supplementary Fig. 8b,c). Furthermore, AMPKα2 triggered HuR eviction from the cytoplasm and induced C/EBPβ phosphorylation on Thr188, which was most apparent in *Cebpb*^{UTR}-expressing cells (Supplementary Fig. 8e). Thus, AMPKα2 converts NIH3T3^{RAS} cells to a phenotype resembling that of senescent MEFs, especially when C/EBPβ is also expressed.

We also tested the consequences of expressing AMPKα2 and/or CaMKKβ in A549 cells. AMPKα2 alone had a potent cytostatic effect that was not further increased by co-expression of CaMKKβ (Fig. 7e). These cells contain detectable levels of endogenous CaMKKβ, which may explain the relatively minor effects of its over-expression, whereas they express very low levels of AMPKα2 (Fig. 7f). AMPK phosphorylation (p-Thr172) was not seen in control cells and was weakly detected in cells expressing AMPKα2 alone, while much higher levels were observed in cells over-expressing both CaMKKβ and AMPKα2. Abundant AMPK levels (detected by a pan-AMPK antibody) were apparent in all cells, indicating that A549 cells express a non-phosphorylated pool of AMPKα1. Thus, the AMPKα1 isoform cannot be phosphorylated by CaMKKβ, whereas this upstream kinase selectively modifies AMPKα2. Accordingly, over-expression of AMPKα2 in A549 cells decreased cytoplasmic HuR levels and induced C/EBPβ phosphorylation, and both effects were enhanced by co-expression of CaMKKβ (Fig. 7g,h).

Down-regulation of AMPKα2 has been reported in breast tumors and other cancers[43,44], suggesting that it has tumor suppressor functions *in vivo*. Therefore, we used a *Kras*^{G12D}-induced mouse lung adenocarcinoma (ADC) model[45] to investigate whether the CaMKKβ-AMPKα2-C/EBPβ pathway is disrupted in these tumors (Fig. 8a). IF staining showed detectable AMPKα2 levels in normal areas of the lung but much lower expression in ADCs (Fig. 8b). CaMKKβ was also significantly reduced in tumor areas. Moreover, p-C/EBPβ (Thr188) was decreased in ADCs relative to normal lung, while total C/EBPβ levels were comparable in both regions, indicating that the activated form of C/EBPβ is diminished in neoplastic cells. We also analyzed benign lung adenomas induced in *LSL-BRAF*^{V600E}/+ mice (Fig. 8a) through intratracheal instillation of Ad.Cre virus[46]. These *BRAF*^{V600E}-dependent tumors displayed reduced levels of AMPKα2, CaMKKβ and p-C/EBPβ compared to normal tissue (Fig. 8c). Thus, both *Kras*- and *BRAF*-driven lung tumorigenesis is associated with disruption of the CaMKKβ-AMPKα2 axis, preventing RAS signaling from activating this pro-senescence pathway. In line with these findings, analysis of AMPKα1 (*PRKAA1*) and AMPKα2 (*PRKAA2*) mRNA expression across a range of human cancers (Oncomine) showed decreased levels of *PRKAA2* in neoplasms such as brain/CNS, gastric, head and neck, and particularly colorectal cancers (Supplementary Fig. 9a). *PRKAA1* was also down-regulated in specific cancers such as breast, but in colorectal cancers *PRKAA2* consistently displayed greater reduction (Supplementary Fig. 9b).

DISCUSSION

Here we identify a novel OIS pathway that involves AMPK as a critical intermediate. We show that AMPKα2, but not AMPKα1, functions as a kinase downstream of oncogenic RAS that elicits nuclear translocation of HuR in primary fibroblasts. Activation of this

pathway decreases the cytoplasmic availability of HuR, thereby dampening the 3′UTR mechanism that suppresses C/EBPβ activity. When active, UPA targets *Cebpb* transcripts to the peripheral cytoplasm, which is physically separate from the perinuclear location of p-ERK and other kinases such as CK2[10,47]. This prevents C/EBPβ phosphorylation, possibly because translation and phosphorylation are tightly coupled. However, AMPK activators such as RAS or metformin reduce cytoplasmic HuR and disrupt peripheral trafficking of *Cebpb* transcripts, causing the mRNA to become pan-cytoplasmic as is seen for transcripts lacking the 3′UTR[10]. Thus, relocation of *Cebpb* transcripts to the perinuclear region allows locally translated C/EBPβ to access p-ERK1/2 and CK2[47], facilitating phosphorylation and functional activation of C/EBPβ.

In primary cells, RAS signals through the AMPKα2-HuR-C/EBPβ axis to elicit growth arrest and senescence. The canonical AMPK pathway triggered by elevated AMP:ATP ratios can also activate C/EBPβ and promote senescence, but this response primarily involves AMPKα1 and remains intact in AMPKα2-deficient cells. As depicted in Fig. 8d, the two AMPKα isoforms have non-overlapping functions, at least with respect to the stimuli investigated here. Our findings support and extend previous studies showing that AMPKα2, but not AMPKα1, suppresses RAS-driven transformation of mouse fibroblasts[36]. Furthermore, it was recently reported that the ubiquitin-conjugating enzyme, UBE2O, is an oncoprotein that targets AMPKα2 but not AMPKα1 for proteasomal degradation in certain cancers[44]. Therefore, AMPKα2 down-regulation achieved through decreased mRNA expression and/or enhanced protein turnover appears to be a key mechanism of senescence bypass in tumor cells.

We found that RAS signaling to AMPK does not involve LKB1 but instead requires the alternative kinase, CaMKKβ. CaMKKβ and calmodulin (CaM) can form a complex with AMPKα[41], although no selectivity for AMPKα isoforms has been reported. This complex also contains the regulatory subunit AMPKβ, but not the γ subunit that binds AMP. As a result, CaMKKβ-AMPK assemblies are unresponsive to AMP and instead are activated by Ca^{++}. Ca^{++} release from the ER is triggered by the lipid second messenger, IP3, and this response can be elicited by RAS activation. Hence, increased Ca^{++} flux could stimulate CaMKKβ-AMPKα2 in cells expressing oncogenic RAS. Accordingly, we found that a Ca^{++} chelator blocks RAS-induced HuR translocation and C/EBPβ activation. The fact that CaMKKβ and AMPKα2 are both down-regulated in cancers underscores their important anti-oncogenic and pro-senescence functions. To our knowledge, this is the first evidence of a tumor suppressor role ascribed to CaMKKβ.

Although our work highlights the anti-oncogenic functions of AMPKα2, Faubert et al.[18] reported that AMPKα1 also has intrinsic tumor suppressor activity in a Myc-driven model of lymphomagenesis. This occurs primarily through the ability of AMPKα1 to inhibit the Warburg effect (a switch to aerobic glycolysis). These findings, together with the fact that LKB1 is frequently lost in RAS tumors, indicate that LKB1-AMPKα1 signaling can negatively regulate tumor initiation or progression. Nonetheless, AMPKα2 levels are down-regulated in many human malignancies and mouse lung tumors. Therefore, we suggest that the anti-oncogenic activity of AMPKα1 primarily involves a response to metabolic stress, most likely involving LKB1 as an upstream regulator. LKB1 loss would facilitate continued

proliferation of tumor cells under conditions of metabolic imbalance. By contrast, AMPKα2 is a specific mediator of RAS signaling and induces a pro-senescence program via targets such as HuR and its effectors, including C/EBPβ. Along with these anti-oncogenic functions, at least low levels of AMPK activity are required for tumor cells to adapt to nutrient-poor and oxygen-deficient environments, and pro-oncogenic roles for AMPK have been reported[48–50]. Thus, tumor suppression by AMPKs and their upstream kinases is complex and is influenced by cellular contexts. Further studies are needed to fully understand how components of the AMPK axis can positively and negatively affect tumorigenesis.

Another difference between the RAS-AMPKα2 and AMP-AMPKα1 axes involves their ability to regulate NF-κB. Canonical AMPK activators such as metformin are known to suppress inflammation by inhibiting one or more nodes in the NF-κB pathway[25–27]. However, oncogenic RAS induces transcription of NF-κB-dependent SASP genes in senescent MEFs despite signaling through AMPKα2, and activates NF-κB in senescent cells[51]. AMPKα2 appears to partially inhibit NF-κB in MEFs undergoing OIS (Supplementary Fig. 6c,d). However, NF-κB activation does occur in these cells and causes SASP induction. It is possible that the low levels of AMPKα2 in MEFs are insufficient to efficiently suppress NF-κB signaling in response to RAS signaling. In any case, our findings underscore the beneficial effects of using AMPK agonists that inhibit NF-κB and suppress inflammation to prevent or treat cancer. We suggest that stimuli that increase cellular AMP levels, such as metformin, exercise and calorie restriction, act primarily through AMPKα1 and not via the CaMKKβ-AMPKα2 axis.

Our data show that reversal of C/EBPβ 3′UTR inhibition (UPA) is an important target of the RAS-CaMKKβ-AMPKα2-HuR pathway. This pathway licenses post-translational activation of C/EBPβ and promotes OIS. Pre-senescent, proliferating MEFs display appreciable cytoplasmic HuR and reduced C/EBPβ activity, conditions that are acutely reversed by oncogenic RAS signaling. Thus, oncogenic RAS activates C/EBPβ and senescence through two separate but convergent effector pathways: CaMKKβ-AMPKα2 overrides C/EBPβ UPA, while the RAF-ERK cascade provides a strong C/EBPβ activating signal (Fig. 8d). In contrast, immortalized cells are resistant to the UPA-cancelling effects of RAS by as yet unknown pathways, possibly linked to loss of tumor suppressors, leading to down-regulation of CaMKKβ and/or AMPKα2.

To date, UPA regulation has only been demonstrated for C/EBPβ, although the *Cebpa* 3′UTR can suppress RAS-induced activation of C/EBPβ when appended to the *Cebpb* coding region[10]. However, it seems unlikely that UPA regulation is unique to C/EBPβ. Conceivably, similar mechanisms could control other pro-senescence regulators, which together may form a tumor suppressor network activated by RAS-CaMKKβ-AMPKα2 signaling. Our findings warrant further studies to identify additional proteins whose anti-oncogenic activities, rather than their expression, are constrained in tumor cells by 3′UTR-dependent mechanisms.

MATERIALS AND METHODS

Animal procedures and preparation of MEFs

Mice were maintained in accordance with National Institutes of Health animal guidelines following protocols approved by the NCI-Frederick Animal Care and Use Committee. Mouse embryonic fibroblasts (MEFs) were prepared from *WT* and *Cebpb*$^{-/-}$ embryos (E13.5)[52]; *Ampka1*$^{-/-}$, *Ampka2*$^{-/-}$ and DKO mice and MEFs have been described[35]. *Lkb1*$^{-/-}$ MEFs[40] were kindly provided by Dr. Nabeel Bardeesy. Primary MEFs were maintained at low passage and were cultured in DMEM (Invitrogen) supplemented with 10% fetal bovine serum (FBS; Gibco) and 100 U/ml penicillin–streptomycin (Gibco) and Primocin (Invivogen). Two mouse lung tumor models were used: *Kras*$^{LA2/+}$ mice[45], which spontaneously develop lung tumors that progress to ADCs, and *LSL-BRAF*$^{V600E/+}$ mice[46], which develop benign adenomas following intratracheal instillation of Ad.Cre virus (7.5×10^6 Pfu/animal; Viral Vector Core Facility, University of Iowa College of Medicine).

Antibodies and reagents

Rabbit antibodies to C/EBPβ (C-19), ERK1 (C-19), NF-κB p65 (C-20), CaMKKβ (H-95) and actin (I-19-R), mouse antibodies to HuR (3A2), C/EBPβ (47A1), C/EBPβ (H7), p-ERK (E-4), Importin α1(B-9), and goat antibody to AMPKα2 (A-20) were purchased from Santa Cruz Biotechnology. Rabbit antibodies to AMPKα (#2532), pAMPKα (#2531), and p-ERK (#4377) were purchased from Cell Signaling Technologies. Rabbit antibody to p-C/EBPβ (T188) was from Abcam (pT235). Rabbit antibody to AMPKα2 (#21494) was from ThermoFisher. Anti-mouse (W4028) and anti-rabbit (W4018) HRP conjugated secondary antibodies were from Promega. Anti-Mouse Alexa® Fluor 488 and anti-rabbit Alexa® Fluor 594 conjugated secondary antibody was from ThermoFisher. Anti-rabbit Alexa® Fluor 647 conjugated secondary antibody was from Abcam. X-tremeGENE HP DNA transfection reagent was from Roche Diagnostics. AICAR was obtained from Cell Signaling Technology, metformin was from Calbiochem, sodium salicylate was from ThermoFisher, STO-609 was from Sigma, and BAPTA was from Abcam.

Cells and cell culture

NIH3T3 cells (American Type Culture Collection) were maintained in DMEM supplemented with 10% calf serum (Colorado Serum Company). A549, MCF7 and HEK-293T cell lines and 293GP2 packaging cells (American Type Culture Collection) were cultured in DMEM supplemented with 10% FBS (Gibco). All media were supplemented with Normocin (InvitroGen) to prevent Mycoplasma contamination. Cell lines were not authenticated. Where appropriate, cells were treated with the indicated doses of AMPK activators AICAR, metformin or sodium salicylate for the specified durations.

Plasmids

An expression plasmid for CA-AMPK[53] was kindly provided by Dr. Rusty Jones (McGill University) and the insert was transferred to pBabe-puro and pWZL-blast. Expression plasmids for mouse C/EBPβ coding region (C/EBPβ$^{\Delta UTR}$) and C/EBPβ coding region plus 3′UTR (C/EBPβ^{UTR}) have been described previously[10]; the genes were transferred to

pBabe-puro and pWZL-blast retroviral vectors. Lentiviral expression vectors for AMPKα2 and CaMKKβ were provided by Dr. Dominic Esposito (FNLCR, Frederick, MD). Lentiviral vectors containing an shRNA construct simultaneously targeting AMPKα1/2 (human and mouse)[54] and a control shRNA vector were kindly provided by Dr. Thomas Brown (Wright State University). Lentiviral shRNA vectors targeting mouse CaMKKβ (#TRCN0000276649), AMPKα1 (#TRCN0000360770) and Importin α1 (#TRCN0000093514) were purchased from Sigma-Aldrich. Human C/EBPβ shRNA and a non-targeting shRNA control in pSuperRetro-neo were described previously[10]. Human $HRAS^{G12V}$ was expressed from pWZL-hygro[6]. Plasmids for retroviral packaging have been described[9]; lentiviral packaging/envelope plasmids pMD2.G (#12259), pMDLg/pRRE (#12251), and pRSV/Rev (#12253) were obtained from Addgene.

Retroviral and lentiviral infections

Retroviral and lentiviral plasmids were transfected into 293GP2 and 293T packaging cell lines, respectively, using standard $CaPO_4$ precipitation. For lentiviral transfection, 20 μg of lentiviral vector, 6 μg of pMD2.G, 10 μg of pMDLg/pRRE and 5 μg of pRSV/Rev were co-transfected into 293T cells. For retroviral transfection, 20 μg of retroviral vector and 4 μg of VSVG plasmids were co-transfected into 293GP2 cells in 10cm dishes. 48–72 h after transfection, viral supernatants were collected every 12 h, pooled, filtered (0.45 mm), supplemented with 8 mg/ml polybrene, and used to infect target cells. Three infections were performed and cells were subjected to the appropriate antibiotic selection. Multiple genes were introduced by sequential infection and drug selection.

Transient transfection and luciferase assays

HEK293T cells were transfected with 200 ng C/EBPβ vector and 100 ng of pcDNA3-$HRAS^{G12V}$ in 60 mm dishes. After transfection, cells were cultured in complete media for 24h and then serum starved overnight prior to harvesting. For transactivation assays, 293T cells were transfected with 100 ng 2× C/EBP-luc reporter and 5 ng C/EBPβ vector with 10 ng pcDNA3-$HRAS^{G12V}$ plasmid. Cells were lysed in 1× passive lysis buffer (Promega) and luciferase activity was measured using a GLOMAX 20/20 luminometer (Promega). Luciferase values were normalized to total protein concentration of the lysate. Data are presented as fold activation of the reporter alone and represent means ±SD of at least three independent experiments.

Growth curves

Retrovirally or lentivirally infected cells were seeded at 2.5×10^4 cells/well in 6-well plates. At the indicated times, cells were washed with phosphate-buffered saline (PBS), fixed in 10% formalin, rinsed with water, stained with 0.1% crystal violet (Sigma) for 30 min, rinsed extensively, and dried. The dye was extracted with 10% acetic acid and absorbance measured at 590 nm. All values were normalized to day 0 (the first day after plating). For proliferation assays in the presence of AMPK activators, cells were treated with metformin (10 mM for MEFs, 1 mM for A549 cells) or sodium salicylate (0.3 mM for MEFs, 3 mM for A549 cells) for the duration of the growth assay. Proliferation was assayed as described above. All growth assays were conducted in triplicate wells.

Colony assays

Cells (MEFs) were seeded at 2.5×10^4 cells/dish in 10 cm dishes. Media was replaced weekly. After two weeks, cells were washed with phosphate-buffered saline (PBS), fixed in 10% acetic acid for 30 min, rinsed with water, stained with 0.4% crystal violet (Sigma) for 30 min, rinsed extensively, and dried. Plates were scanned and colonies counted on the images. The assays were performed in duplicate.

Senescence-associated β-galactosidase (SA-β-gal) assay

WT and *Cebpb*$^{-/-}$ MEFs (passage 2–4) were plated at 5×10^4 cells per well in 6-well plates and cultured for 3–4 days. Cells were fixed and stained (Senescence Detection Kit; Calbiochem) according to the manufacturer's instructions with the following modification: the staining solution was titrated with 2M HCl to reduce the pH below 6.0 to optimize SA-βgal staining in mouse cells. SA-β-gal stained cells were counted by acquiring at least four fields using 10× bright field microscopy, and are expressed as a percentage of the total cells scored.

mRNA localization

The GFP-MS2-nls reporter system has been described previously[55]. pcDNA-*Cebpb*^{UTR}-Ms2b and pcDNA-*Cebpb*$^{\Delta UTR}$-Ms2b vectors were generated by inserting the array of MS2 binding sites from the RSV-lacZ-MS2b vector[55] immediately downstream of the *Cebpb* coding region, as described[10]. NIH3T3 cells were plated at 5×10^4 cells/35mm dish and transfected with 200 ng GFP-MS2-nls reporter plasmid and 2.3 μg of the *Cebpb*-Ms2b vector using Polyfect (Qiagen) following the manufacturer's instructions. After 36 hr, the cells were stained with 1 μg/ml DAPI (Sigma). Fluorescence images of unfixed/live cells were taken with a Zeiss LCI-510 confocal microscope.

RNA FISH

Cells were seeded on μ-Slides VI$^{0.4}$ (Ibidi). Forty-eight hours after plating, the cells were washed in Cytoskeleton Buffer (CB)[56] (10 mM MES pH 6.1, 150 mM NaCl, 5 mM $MgCl_2$, 5 mM EGTA, 5 mM glucose) and permeabilized in ice-cold Pre-Fixative mix[57] (2% paraformaldehyde, 0.01% glutaraldehyde, 0.05% saponin, in CB) for 15 min at 4°C. Cells were then fixed with ice-cold Fixative mix (2% paraformaldehyde, 0.01% glutaraldehyde, in CB) for 100 min at 4°C. The cells were washed with CB twice and fixative was quenched by addition of 50 mM NH_4Cl for 5 min at 20°C. For the RNA fluorescence *in situ* hybridization (FISH) procedure, probe hybridization, signal amplification and post-hybridization washes were performed using the QuantiGene ViewRNA ISH Cell Assay (Affymetrix) according to the manufacturer's protocol. A human *CEBPB* probe (VA1-18129) or mouse *Cebpb* probe (VB1-10094) was used.

Cell segmentation and RNA FISH data analysis

The nucleus and cell membrane boundary were segmented and identified using Graphcut algorithm developed previously[58]. Briefly, a point on the cell was first selected that performs a polar transform of a circular area surrounding the cell. Next, the algorithm calculates a gradient image of the transform and creates a source-sink directed graph of the image using

the pixels as nodes and their gradient values as edges. A max-flow mincut then segments the cartesian image. Finally, the algorithm reconverts the image to cartesian coordinates. In addition, the user can modify any local segmentation that was inaccurate; the addition of this point increases the edge strength of that pixel on the polar graph and corrects the segmentation. The localization of mRNA single molecule image was determined using two dimensional Gaussian-fitting by ThunderSTORM[59]. The number and percentage of localizations were quantified in three distinct regions of the cell using a home-built algorithm in Matlab (Split_region.m). The script utilizes a euclidean distance transform (EDT) to generate the distance from each pixel to the boundaries of the cell and nucleus. The “inner region” was defined as the area within the cell whose pixels are at least twice as close to the nucleus as they are to the cell boundary (plasma membrane), excluding the nucleus. The “intermediate region” encompasses everything excluding the inner and out regions and the nucleus. The “outer region” contains pixels that are at least twice as close to the cell boundaries than the nuclear boundaries. The proportion of localizations in each region was then calculated, with any localizations within the nucleus removed from the total.

Code availability

Graphcut and Split_region.m software is freely available upon request.

Immunofluorescence

After RNA FISH, immunofluorescence was performed by incubating cells with HuR (1:400) and p-ERK (1:100) primary antibodies for 16 hrs at 4°C in 5% albumin in PBS-S (PBS containing 0.05% Saponin). Cells were washed three times for 5 min at 20°C with PBS-S and incubated for 1 hr at 20°C with Alexa 488- and Alexa 647-conjugated secondary antibodies (1:1000) in 5% albumin in PBS-S. Cells were washed four times with PBS-S for 5 min at 20°C and co-stained with 0.1 μg/mL DAPI (in PBS) for 1 min at 20°C. Cells were washed twice with PBS, and images were acquired using a Zeiss LSM-780 confocal microscope. For other immunofluorescence experiments, 2.5×10^4 cells were plated in glass-bottomed chambers (LabTek) and fixed with ice-cold methanol for 20 min at -20°C. Cells were incubated with respective primary antibodies (1:100) overnight at 4°C in PBS with 5% Normal Goat Serum (Cell Signaling) and 0.1% TritonX100 (Sigma). Following four washes with PBS containing 1% BSA and 0.1% TritonX100, cells were incubated with Alexa 488 and Alexa 594 conjugated secondary antibodies (1:1000) for 1 hr at RT. After five washes, cells were stained with 0.1 μg/mL DAPI in PBS for 15 min at RT followed by two washes with PBS. Fluorescence images were taken with a Zeiss LSM-710 confocal microscope.

Quantitative image analysis

Fluorescence image analysis was performed using Image J software. To quantify cytoplasmic HuR levels, the nuclear fluorescence intensity was subtracted from the total fluorescence for each cell. The mean cytoplasmic intensity was determined and used for further statistical analysis. For C/EBPβ, only nuclear fluorescence intensities were measured. p-C/EBPβ:total C/EBPβ ratios were calculated for individual cells and then averaged.

Immunoblotting

Cells were harvested after washing twice with cold (4°C) PBS. The cells were lysed with low salt buffer (20 mM HEPES pH 7.9, 0.1 mM EDTA, 10 mM NaCl, 0.1% NP-40) on ice for 10 min. Nuclei were harvested by centrifugation at 3500 rpm for 10 min, and the supernatant was used as cytoplasmic fraction. Nuclei were lysed with high salt buffer (20 mM HEPES pH 7.9, 0.2 mM EDTA, 420 mM NaCl, 25% glycerol) at 4°C for 30 min with vigorous shaking. Nuclear debris was pelleted by centrifugation at 14,000 rpm for 5 min, and the supernatant was used for further experiments or stored at −70°C. For whole cell extracts, cells were lysed in medium salt buffer (50 mM Tris-HCl pH 7.4, 150 mM NaCl, 1 mM EDTA, 1% NP-40, 0.1% SDS, 0.5% sodium deoxycholate) on ice for 10 min with intermittent vortexing. Cellular debris was pelleted by centrifugation at 14,000 rpm for 10 min and supernatant was collected for further analysis. All buffers were supplemented with a protease and phosphatase inhibitor cocktail (Calbiochem). Protein samples (20–50μg) were resolved by electrophoresis on 10% or 12% Mini-PROTEAN TGX Precast Gels (Biorad) and electrophoretically transferred to PVDF membranes. The blots were probed with the appropriate primary antibodies, followed by goat anti-rabbit IgG or goat anti-mouse IgG conjugated to horseradish peroxidase and visualized using the enhanced chemiluminescence method (ThermoFisher).

Electrophoretic mobility shift assays (EMSA)

EMSA was performed essentially as described[60]. Briefly, a dsDNA probe containing a consensus C/EBP site was end-labeled with [^{32}P]dATP (Amersham) and polynucleotidylkinase (Roche). DNA-binding assays were carried out in a 25 μl reaction containing 5–10 μg nuclear extract, 20 mM HEPES (pH 7.9), 200 mM NaCl, 5% Ficoll, 1 mM EDTA, 50 mM DTT, 0.01% Nonidet P-40, 1.75 μg poly(dI-dC), and 2×10^4 cpm probe. After incubation at room temperature for 20 min, 10–15 μl of the binding reaction was loaded onto a 6% polyacrylamide gel in TBE (90 mM Tris base, 90 mM boric acid, 0.5 mM EDTA) buffer and electrophoresed at 160 V for 2 h. Supershift assays were carried out by pre-incubating the nuclear extract with 1 μl of the appropriate antibody at 4°C for 30 min before adding the binding reaction mixture.

RNA isolation and RT-qPCR

Total RNA was prepared using the GeneJet RNA Purification kit (ThermoFisher). Reverse transcription followed by quantitative PCR (RT-qPCR) was used to measure mRNA expression levels. 100–1000 ng of total RNA was reverse transcribed using Maxima First Strand cDNA Synthesis kit (ThermoFisher) according to the manufacturer's protocol. The resulting cDNA was analyzed by quantitative PCR using SsoAdvanced SYBR Green Supermix (Bio-Rad) in the CFX96 Real Time PCR System (Bio-Rad). The primers for *Il1a*, *Il1b*, *Il6*, *Cxcl1*, *Cxcl2*, *Ccr1* and *Ppia* were obtained from Qiagen. Primers for *Prkaa1* and *Prkaa2* were obtained from Bio-Rad. All samples were assayed in triplicate and normalized to control values in the same samples. The housekeeping gene Ppia was used as an internal standard.

Statistical analysis

Statistical significance was calculated using Student's t test and ANOVA. ANOVA was performed using SPSS and Student's *t* test was performed using GraphPad Prism 7. p values less than 0.05 were considered to be significant. For growth assays in MEFs, individual experiments were excluded from the study if RAS-induced growth arrest was not observed in the *WT* group. For SASP gene expression studies, individual experiments were excluded from the analysis if induction by RAS was not statistically significant in the *WT* MEF group.

Supplementary Material

Refer to Web version on PubMed Central for supplementary material.

Acknowledgments

We thank R. Jones for the CA-AMPK vector, N. Bardeesy for *Lkb1*$^{-/-}$ MEFs, T. Brown for a pan-AMPKα knockdown vector, K. Saylor and N. Martin for animal husbandry and genotyping, and A. Kane (Scientific Publications, Graphics & Media, Leidos Biomedical Research, Inc., Frederick National Laboratory for Cancer Research) for preparation of figures. This research was supported by the Intramural Research Program of the NIH, National Cancer Institute, Center for Cancer Research. The content of this publication does not necessarily reflect the views or policies of the Department of Health and Human Services, nor does mention of trade names, commercial products, or organizations imply endorsement by the U.S. Government.

References

1. Campisi J. Senescent cells, tumor suppression, and organismal aging: good citizens, bad neighbors. Cell. 2005; 120:513–522. [PubMed: 15734683]
2. Kuilman T, Michaloglou C, Mooi WJ, Peeper DS. The essence of senescence. Genes Dev. 2010; 24:2463–2479. [PubMed: 21078816]
3. Coppe J-P, Desprez P-Y, Krtolica A, Campisi J. The Senescence-Associated Secretory Phenotype: The Dark Side of Tumor Suppression. Annual Review of Pathology: Mechanisms of Disease. 2010; 5:99–118.
4. Nakajima T, Kinoshita S, Sasagawa T, Sasaki K, Naruto M, Kishimoto T, et al. Phosphorylation at threonine-235 by a ras-dependent mitogen-activated protein kinase cascade is essential for transcription factor NF-IL6. Proc Natl Acad Sci USA. 1993; 90:2207–2211. [PubMed: 8384717]
5. Lee S, Shuman JD, Guszczynski T, Sakchaisri K, Sebastian T, Copeland TD, et al. RSK-mediated phosphorylation in the C/EBP{beta} leucine zipper regulates DNA binding, dimerization, and growth arrest activity. Mol Cell Biol. 2010; 30:2621–2635. [PubMed: 20351173]
6. Sebastian T, Malik R, Thomas S, Sage J, Johnson PF. C/EBPbeta cooperates with RB:E2F to implement Ras(V12)-induced cellular senescence. EMBO J. 2005; 24:3301–3312. [PubMed: 16107878]
7. Kuilman T, Michaloglou C, Vredeveld LC, Douma S, van Doorn R, Desmet CJ, et al. Oncogene-induced senescence relayed by an interleukin-dependent inflammatory network. Cell. 2008; 133:1019–1031. [PubMed: 18555778]
8. Rodier F, Coppe JP, Patil CK, Hoeijmakers WA, Munoz DP, Raza SR, et al. Persistent DNA damage signalling triggers senescence-associated inflammatory cytokine secretion. Nat Cell Biol. 2009; 11:973–979. [PubMed: 19597488]
9. Huggins CJ, Malik R, Lee S, Salotti J, Thomas S, Martin N, et al. C/EBPgamma suppresses senescence and inflammatory gene expression by heterodimerizing with C/EBPbeta. Mol Cell Biol. 2013; 33:3242–3258. [PubMed: 23775115]
10. Basu SK, Malik R, Huggins CJ, Lee S, Sebastian T, Sakchaisri K, et al. 3′UTR elements inhibit Ras-induced C/EBPbeta post-translational activation and senescence in tumour cells. EMBO J. 2011; 30:3714–3728. [PubMed: 21804532]

11. Kim HH, Gorospe M. Phosphorylated HuR shuttles in cycles. Cell Cycle. 2008; 7:3124–3126. [PubMed: 18927508]
12. Doller A, Pfeilschifter J, Eberhardt W. Signalling pathways regulating nucleo-cytoplasmic shuttling of the mRNA-binding protein HuR. Cell Signal. 2008; 20:2165–2173. [PubMed: 18585896]
13. Lopez de Silanes I, Lal A, Gorospe M. HuR: post-transcriptional paths to malignancy. RNA Biol. 2005; 2:11–13. [PubMed: 17132932]
14. Yoo PS, Sullivan CA, Kiang S, Gao W, Uchio EM, Chung GG, et al. Tissue microarray analysis of 560 patients with colorectal adenocarcinoma: high expression of HuR predicts poor survival. Ann Surg Oncol. 2009; 16:200–207. [PubMed: 19009247]
15. Wang W, Caldwell MC, Lin S, Furneaux H, Gorospe M. HuR regulates cyclin A and cyclin B1 mRNA stability during cell proliferation. EMBO J. 2000; 19:2340–2350. [PubMed: 10811625]
16. Hardie DG. AMP-activated protein kinase: an energy sensor that regulates all aspects of cell function. Genes Dev. 2011; 25:1895–1908. [PubMed: 21937710]
17. Mihaylova MM, Shaw RJ. The AMPK signalling pathway coordinates cell growth, autophagy and metabolism. Nat Cell Biol. 2011; 13:1016–1023. [PubMed: 21892142]
18. Faubert B, Boily G, Izreig S, Griss T, Samborska B, Dong Z, et al. AMPK is a negative regulator of the Warburg effect and suppresses tumor growth in vivo. Cell Metab. 2013; 17:113–124. [PubMed: 23274086]
19. Shackelford DB, Shaw RJ. The LKB1-AMPK pathway: metabolism and growth control in tumour suppression. Nat Rev Cancer. 2009; 9:563–575. [PubMed: 19629071]
20. Wang W, Yang X, Lopez de Silanes I, Carling D, Gorospe M. Increased AMP:ATP ratio and AMP-activated protein kinase activity during cellular senescence linked to reduced HuR function. J Biol Chem. 2003; 278:27016–27023. [PubMed: 12730239]
21. Wang W, Fan J, Yang X, Furer-Galban S, Lopez de Silanes I, von Kobbe C, et al. AMP-activated kinase regulates cytoplasmic HuR. Mol Cell Biol. 2002; 22:3425–3436. [PubMed: 11971974]
22. Wang W, Yang X, Kawai T, Lopez de Silanes I, Mazan-Mamczarz K, Chen P, et al. AMP-activated protein kinase-regulated phosphorylation and acetylation of importin alpha1: involvement in the nuclear import of RNA-binding protein HuR. J Biol Chem. 2004; 279:48376–48388. [PubMed: 15342649]
23. Sebastian T, Johnson PF. RasV12-mediated down-regulation of CCAAT/Enhancer Binding Protein {beta} in immortalized fibroblasts requires loss of p19Arf and facilitates bypass of oncogene-induced senescence. Cancer Research. 2009; 69:2588–2598. [PubMed: 19276382]
24. Salotti J, Sakchaisri K, Tourtellotte WG, Johnson PF. An Arf-Egr-C/EBPbeta pathway linked to ras-induced senescence and cancer. Mol Cell Biol. 2015; 35:866–883. [PubMed: 25535333]
25. Salminen A, Hyttinen JM, Kaarniranta K. AMP-activated protein kinase inhibits NF-kappaB signaling and inflammation: impact on healthspan and lifespan. Journal of molecular medicine. 2011; 89:667–676. [PubMed: 21431325]
26. O'Neill LA, Hardie DG. Metabolism of inflammation limited by AMPK and pseudo-starvation. Nature. 2013; 493:346–355. [PubMed: 23325217]
27. Moiseeva O, Deschenes-Simard X, St-Germain E, Igelmann S, Huot G, Cadar AE, et al. Metformin inhibits the senescence-associated secretory phenotype by interfering with IKK/NF-kappaB activation. Aging Cell. 2013; 12:489–498. [PubMed: 23521863]
28. Bertrand E, Chartrand P, Schaefer M, Shenoy SM, Singer RH, Long RM. Localization of ASH1 mRNA particles in living yeast. Molecular cell. 1998; 2:437–445. [PubMed: 9809065]
29. Foretz M, Guigas B, Bertrand L, Pollak M, Viollet B. Metformin: from mechanisms of action to therapies. Cell Metab. 2014; 20:953–966. [PubMed: 25456737]
30. Hawley SA, Fullerton MD, Ross FA, Schertzer JD, Chevtzoff C, Walker KJ, et al. The ancient drug salicylate directly activates AMP-activated protein kinase. Science. 2012; 336:918–922. [PubMed: 22517326]
31. Shen CH, Yuan P, Perez-Lorenzo R, Zhang Y, Lee SX, Ou Y, et al. Phosphorylation of BRAF by AMPK impairs BRAF-KSR1 association and cell proliferation. Mol Cell. 2013; 52:161–172. [PubMed: 24095280]

32. Kim HH, Abdelmohsen K, Lal A, Pullmann R Jr, Yang X, Galban S, et al. Nuclear HuR accumulation through phosphorylation by Cdk1. Genes Dev. 2008; 22:1804–1815. [PubMed: 18593881]
33. Gwinn DM, Shackelford DB, Egan DF, Mihaylova MM, Mery A, Vasquez DS, et al. AMPK phosphorylation of raptor mediates a metabolic checkpoint. Molecular cell. 2008; 30:214–226. [PubMed: 18439900]
34. Inoki K, Zhu T, Guan KL. TSC2 mediates cellular energy response to control cell growth and survival. Cell. 2003; 115:577–590. [PubMed: 14651849]
35. Laderoute KR, Amin K, Calaoagan JM, Knapp M, Le T, Orduna J, et al. 5′-AMP-activated protein kinase (AMPK) is induced by low-oxygen and glucose deprivation conditions found in solid-tumor microenvironments. Mol Cell Biol. 2006; 26:5336–5347. [PubMed: 16809770]
36. Phoenix KN, Devarakonda CV, Fox MM, Stevens LE, Claffey KP. AMPKalpha2 Suppresses Murine Embryonic Fibroblast Transformation and Tumorigenesis. Genes & cancer. 2012; 3:51–62. [PubMed: 22893790]
37. Wang S, Song P, Zou MH. Inhibition of AMP-activated protein kinase alpha (AMPKalpha) by doxorubicin accentuates genotoxic stress and cell death in mouse embryonic fibroblasts and cardiomyocytes: role of p53 and SIRT1. J Biol Chem. 2012; 287:8001–8012. [PubMed: 22267730]
38. Woods A, Johnstone SR, Dickerson K, Leiper FC, Fryer LG, Neumann D, et al. LKB1 is the upstream kinase in the AMP-activated protein kinase cascade. Curr Biol. 2003; 13:2004–2008. [PubMed: 14614828]
39. Hawley SA, Boudeau J, Reid JL, Mustard KJ, Udd L, Makela TP, et al. Complexes between the LKB1 tumor suppressor, STRAD alpha/beta and MO25 alpha/beta are upstream kinases in the AMP-activated protein kinase cascade. Journal of biology. 2003; 2:28. [PubMed: 14511394]
40. Bardeesy N, Sinha M, Hezel AF, Signoretti S, Hathaway NA, Sharpless NE, et al. Loss of the Lkb1 tumour suppressor provokes intestinal polyposis but resistance to transformation. Nature. 2002; 419:162–167. [PubMed: 12226664]
41. Anderson KA, Ribar TJ, Lin F, Noeldner PK, Green MF, Muehlbauer MJ, et al. Hypothalamic CaMKK2 contributes to the regulation of energy balance. Cell Metab. 2008; 7:377–388. [PubMed: 18460329]
42. Hawley SA, Pan DA, Mustard KJ, Ross L, Bain J, Edelman AM, et al. Calmodulin-dependent protein kinase kinase-beta is an alternative upstream kinase for AMP-activated protein kinase. Cell Metab. 2005; 2:9–19. [PubMed: 16054095]
43. Fox MM, Phoenix KN, Kopsiaftis SG, Claffey KP. AMP-Activated Protein Kinase alpha 2 Isoform Suppression in Primary Breast Cancer Alters AMPK Growth Control and Apoptotic Signaling. Genes & cancer. 2013; 4:3–14. [PubMed: 23946867]
44. Vila IK, Yao Y, Kim G, Xia W, Kim H, Kim SJ, et al. A UBE2O-AMPKalpha2 Axis that Promotes Tumor Initiation and Progression Offers Opportunities for Therapy. Cancer Cell. 2017; 31:208–224. [PubMed: 28162974]
45. Johnson L, Mercer K, Greenbaum D, Bronson RT, Crowley D, Tuveson DA, et al. Somatic activation of the K-ras oncogene causes early onset lung cancer in mice. Nature. 2001; 410:1111–1116. [PubMed: 11323676]
46. Dankort D, Filenova E, Collado M, Serrano M, Jones K, McMahon M. A new mouse model to explore the initiation, progression, and therapy of BRAFV600E-induced lung tumors. Genes Dev. 2007; 21:379–384. [PubMed: 17299132]
47. Basu SK, Lee S, Salotti J, Basu S, Sakchaisri K, Xiao Z, et al. Oncogenic RAS-Induced Perinuclear Signaling Complexes Requiring KSR1 Regulate Signal Transmission to Downstream Targets. Cancer Research. 2017
48. Jeon SM, Hay N. The dark face of AMPK as an essential tumor promoter. Cellular logistics. 2012; 2:197–202. [PubMed: 23676995]
49. Jeon SM, Chandel NS, Hay N. AMPK regulates NADPH homeostasis to promote tumour cell survival during energy stress. Nature. 2012; 485:661–665. [PubMed: 22660331]

50. Rios M, Foretz M, Viollet B, Prieto A, Fraga M, Costoya JA, et al. AMPK activation by oncogenesis is required to maintain cancer cell proliferation in astrocytic tumors. Cancer Research. 2013; 73:2628–2638. [PubMed: 23370326]
51. Chien Y, Scuoppo C, Wang X, Fang X, Balgley B, Bolden JE, et al. Control of the senescence-associated secretory phenotype by NF-kappaB promotes senescence and enhances chemosensitivity. Genes Dev. 2011; 25:2125–2136. [PubMed: 21979375]
52. Sterneck E, Tessarollo L, Johnson PF. An essential role for C/EBPβ in female reproduction. Genes Dev. 1997; 11:2153–2162. [PubMed: 9303532]
53. Jones RG, Plas DR, Kubek S, Buzzai M, Mu J, Xu Y, et al. AMP-activated protein kinase induces a p53-dependent metabolic checkpoint. Mol Cell. 2005; 18:283–293. [PubMed: 15866171]
54. Tangeman L, Wyatt CN, Brown TL. Knockdown of AMP-activated protein kinase alpha 1 and alpha 2 catalytic subunits. J RNAi Gene Silencing. 2012; 8:470–478. [PubMed: 23316259]
55. Rook MS, Lu M, Kosik KS. CaMKIIalpha 3′ untranslated region-directed mRNA translocation in living neurons: visualization by GFP linkage. J Neurosci. 2000; 20:6385–6393. [PubMed: 10964944]
56. Scheffler JM, Schiefermeier N, Huber LA. Mild fixation and permeabilization protocol for preserving structures of endosomes, focal adhesions, and actin filaments during immunofluorescence analysis. Methods Enzymol. 2014; 535:93–102. [PubMed: 24377919]
57. Whelan DR, Bell TD. Image artifacts in single molecule localization microscopy: why optimization of sample preparation protocols matters. Scientific reports. 2015; 5:7924. [PubMed: 25603780]
58. Nandy K, Chellappa R, Kumar A, Lockett SJ. Segmentation of Nuclei From 3D Microscopy Images of Tissue via Graphcut Optimization. IEEE Journal of Selected Topics in Signal Processing. 2016; 10:140–150.
59. Ovesny M, Krizek P, Borkovec J, Svindrych Z, Hagen GM. ThunderSTORM: a comprehensive ImageJ plug-in for PALM and STORM data analysis and super-resolution imaging. Bioinformatics. 2014; 30:2389–2390. [PubMed: 24771516]
60. Parkin SE, Baer M, Copeland TD, Schwartz RC, Johnson PF. Regulation of CCAAT/enhancer-binding protein (C/EBP) activator proteins by heterodimerization with C/EBPgamma (Ig/EBP). J Biol Chem. 2002; 277:23563–23572. [PubMed: 11980905]
61. Descombes P, Schibler U. A liver-enriched transcriptional activator protein, LAP, and a transcriptional inhibitory protein, LIP, are translated from the same mRNA. Cell. 1991; 67:569–579. [PubMed: 1934061]
62. Nakajima K, Kusafuka T, Takeda T, Fujitani Y, Nakae K, Hirano T. Identification of a novel interleukin-6 response element containing an Ets-binding site and a CRE-like site in the *jun*B promoter. Mol Cell Biol. 1993; 13:3027–3041. [PubMed: 8386318]

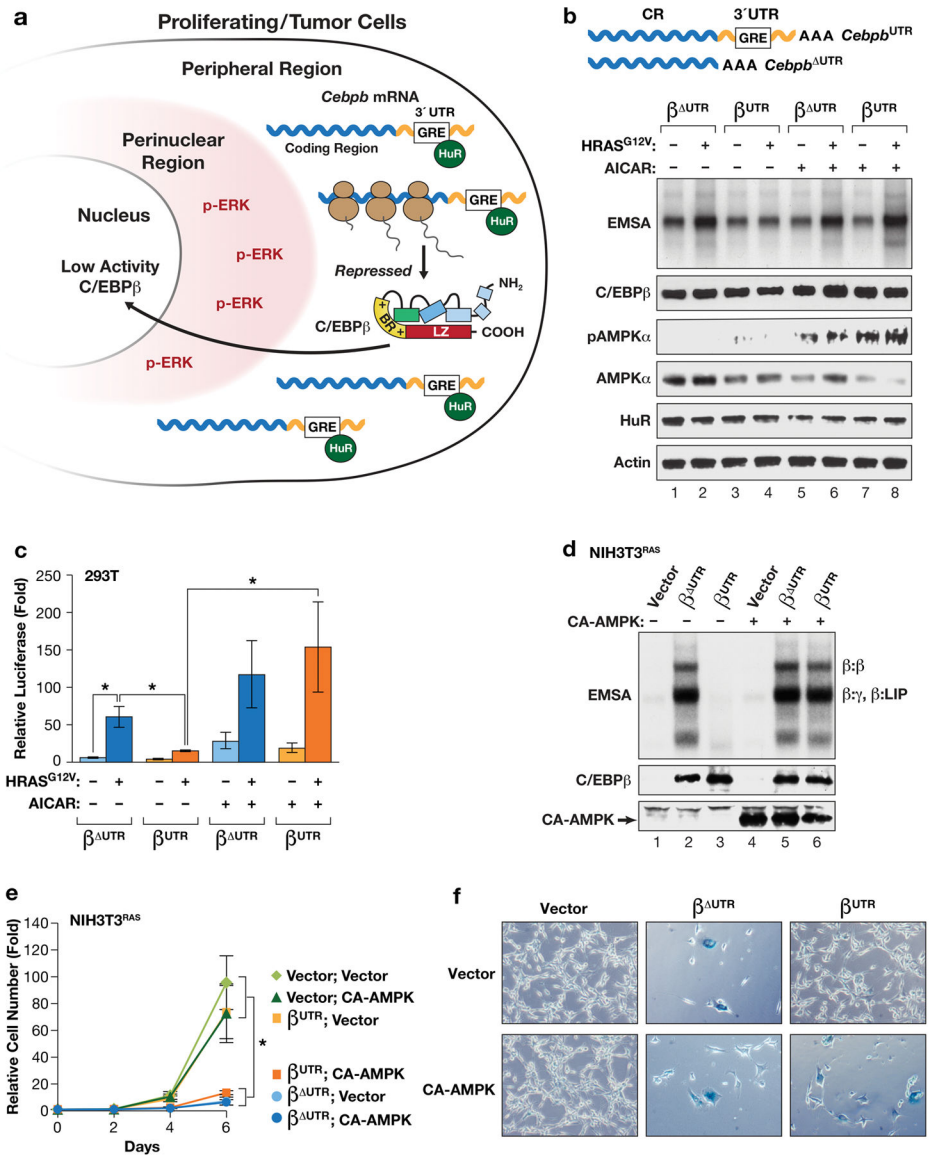

Figure 1.

AMPK signaling abrogates 3′UTR inhibition of RAS-induced C/EBPβ activation. **(a)** Model depicting "3′UTR regulation of protein activity" (UPA)[10] in proliferating and transformed cells. The UPA mechanism involves mutually exclusive localization of *Cebpb* mRNAs (in the peripheral cytoplasm) and the C/EBPβ kinase, activated ERK1/2 (p-ERK) (in the perinuclear cytoplasm). **(b, c)** The AMPK agonist AICAR overrides UPA to activate C/EBPβ. The effect of AICAR on C/EBPβ DNA binding **(b)** and transactivation **(c)** was analyzed in HEK293 cells. Cells were transfected with C/EBPβ constructs containing or lacking the *Cebpb* 3′UTR (β^{UTR} and $\beta^{\Delta UTR}$, respectively), without or with $HRAS^{G12V}$, and treated with vehicle or 1 mM AICAR for 16 hr prior to harvest. In **(b)**, nuclear extracts normalized for C/EBPβ levels were analyzed by EMSA using a consensus C/EBP probe. The image was cropped to remove the top and bottom (free probe) portions of the gel. In **(c)**, transactivation assays were performed using a C/EBP reporter, 2XC/EBP-Luc. Luciferase

activity, normalized to total protein in each lysate, is plotted as fold increase over the reporter alone. n=3; error bars represent S.E.M. Statistical differences between groups were determined by Student's two-tailed t test; *p<0.05. **(d)** Expression of a constitutively active AMPKα1 catalytic subunit (CA-AMPK) reverses UPA inhibition of C/EBPβ DNA binding in RAS-transformed NIH3T3 cells. NIH3T3^{RAS} cells, which express low levels of endogenous C/EBPβ^{23}, were infected with retroviruses expressing β^{UTR} or β$^{\Delta UTR}$, without or with CA-AMPK, and assayed for C/EBPβ DNA binding by EMSA. The various C/EBPβ dimeric complexes are indicated. γ: C/EBPγ; LIP is a truncated translational isoform of C/EBPβ^{61}. **(e)** The same cells were analyzed for proliferation over a 6-day time course. n=3; error bars represent S.E.M. Statistical differences between groups were determined by Student's t test; *p<0.05. **(f)** The cells were also stained for the senescence marker, SA-β-Gal. The proportion of SA-β-Gal^{+} cells in each population is shown in Supplementary Fig. 1c.

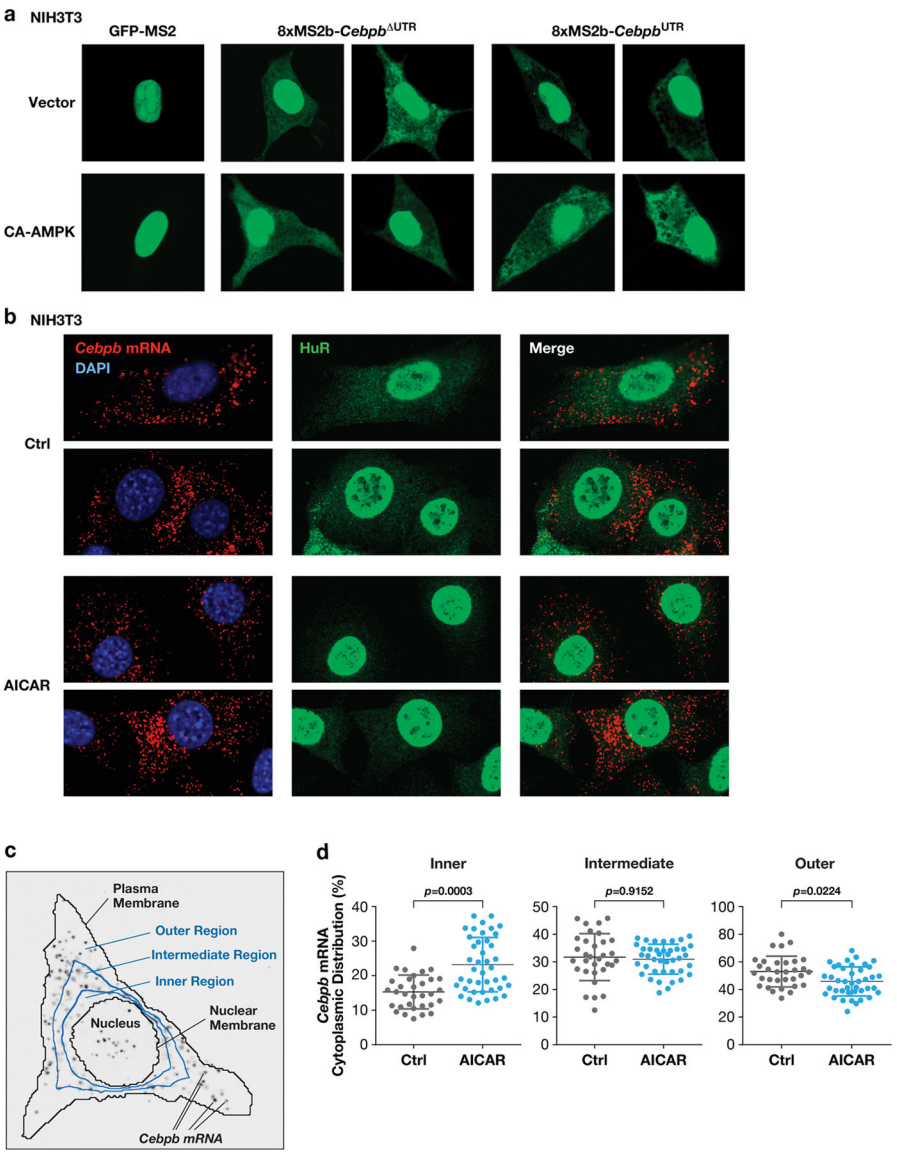

Figure 2.

AMPK signaling decreases cytoplasmic HuR levels and disrupts peripheral localization of *Cebpb* transcripts. **(a)** NIH3T3 cells were transfected with the MS2-GFP-nls reporter alone or together with MS2 binding site-tagged *Cebpb*$^{\Delta UTR}$ or *Cebpb*^{UTR} vectors, ±CA-AMPK. After 42 hr, cells were analyzed by confocal fluorescence microscopy to visualize cytoplasmic distribution of the transcripts. **(b)** Localization of endogenous *Cebpb* mRNA in NIH3T3 cells using RNA FISH. Control and AICAR treated cells were analyzed by FISH using a *Cebpb* hybridization probe. The cells were also immunostained for HuR. **(c)** Scheme for quantification of *Cebpb* mRNA distribution. The cytoplasm was segmented into inner, intermediate, and outer regions by dividing the nuclear-plasma membrane distance radially into thirds. The proportion of the total RNA FISH signal in the three regions was determined for each cell analyzed. **(d)** Quantitative data from the experiment of panel **(b)** are shown in

the scatter plots. n=32 control cells, 41 AICAR-treated cells. Statistical significance was calculated using Student's two-tailed t test; *$p<0.05$.

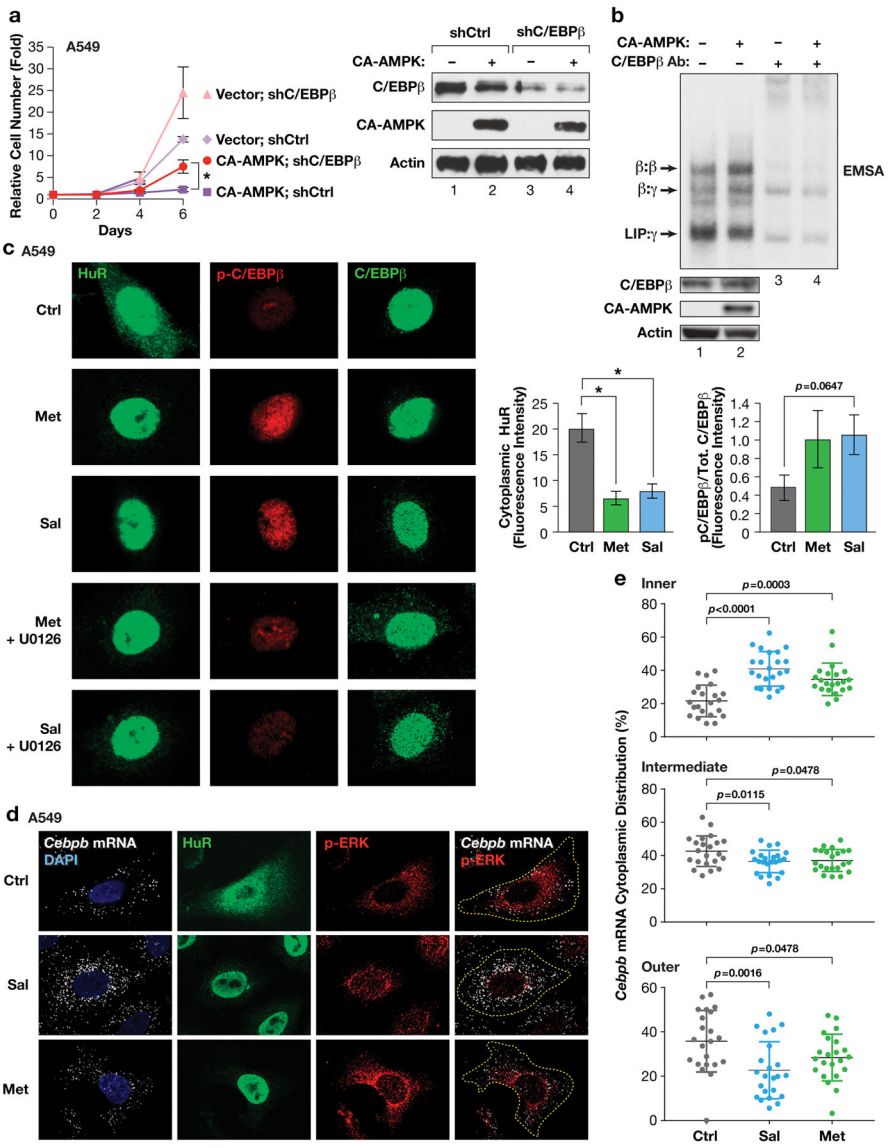

Figure 3.

AMPK signaling activates C/EBPβ in human tumor cells by negatively regulating the HuR-UPA pathway. **(a)** CA-AMPK induces proliferation arrest in A549 lung adenocarcinoma cells that is partially dependent on C/EBPβ. CA-AMPK was expressed with control or C/EBPβ knockdown vectors and cell proliferation was analyzed over a time course. Levels of CA-AMPK and C/EBPβ were determined by immunoblotting (right panel). n=2 experiments, assayed in triplicate; error bars represent S.E.M. Statistical differences between groups were determined by Student's t test; *p<0.05. **(b)** Activated AMPK stimulates C/EBPβ DNA binding and homodimerization in A549 cells. Nuclear extracts from control and CA-AMPK-expressing cells were analyzed by EMSA. C/EBPβ protein levels were normalized in the EMSA reactions so that changes in intrinsic binding activity could be assessed. C/EBPβ-containing complexes were identified by antibody supershift assays (lanes 3–4). **(c)** The AMPK activators metformin and salicylate induce HuR nuclear translocation

and increased phosphorylation on C/EBPβ Thr235 in A549 cells. Right panels show quantification of HuR cytoplasmic intensity and p-C/EBPβ:total C/EBPβ levels in control and drug-treated cells. n=5 cells; statistical significance was calculated using Student's two-tailed t test; *p<0.05. **(d)** *CEBPB* transcripts are excluded from the perinuclear region in A549 cells but become more uniformly distributed following metformin or salicylate treatment. mRNAs were visualized by RNA FISH; the cells were also immunostained for p-ERK and HuR. **(e)** Cytoplasmic *CEBPB* mRNA distribution in cells described in panel **(d)** was quantified as detailed in Fig. 2. n=22 control cells, 23 salicylate-treated cells, 22 metformin-treated cells. Statistical significance was calculated using Student's two-tailed t test; *p<0.05.

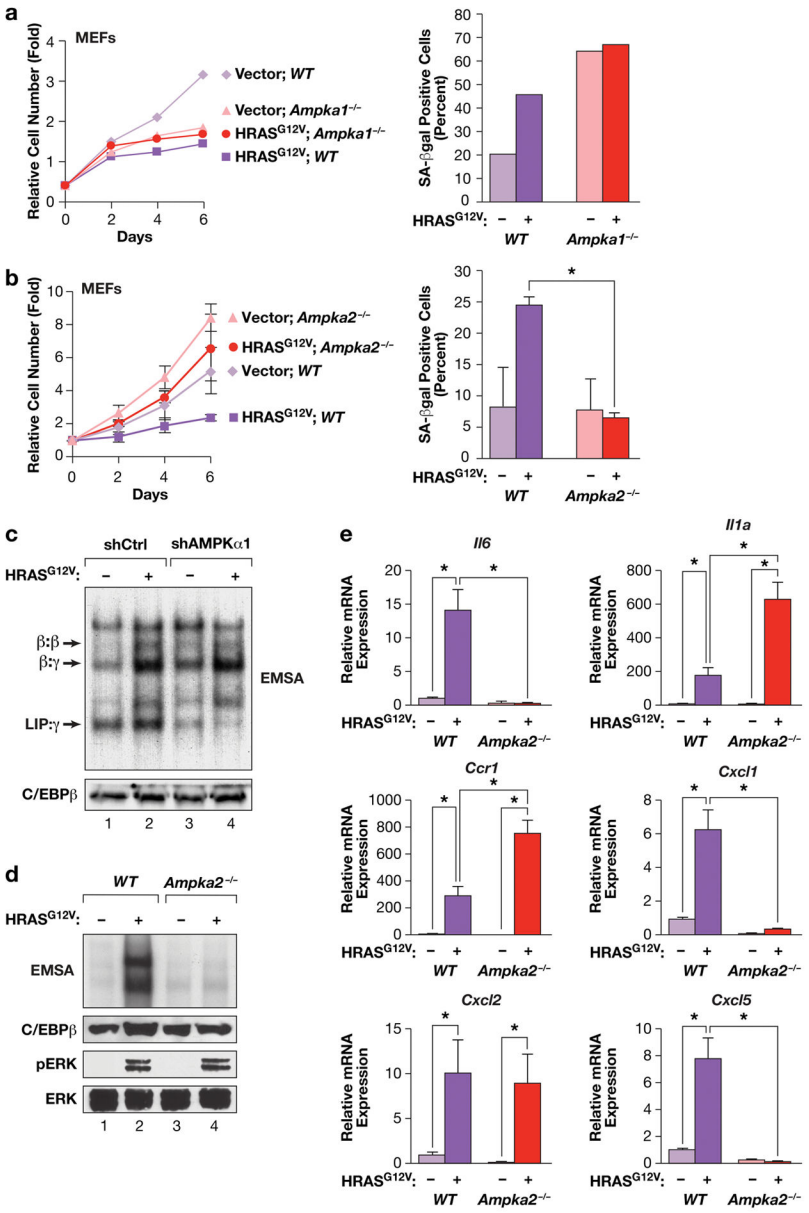

Figure 4.

HRAS^{G12V}-induced senescence and C/EBPβ activation in MEFs is dependent on AMPKα2. **(a)** RAS-induced growth arrest and senescence is independent of AMPKα1 but requires AMPKα2. *WT* and *Ampka1*$^{-/-}$ MEFs were infected with control or HRAS^{G12V}-expressing retroviruses, and cell proliferation (left panel) and senescence (SA-β-Gal staining, right panel) were analyzed. n=1 experiment. **b)** RAS-induced growth arrest and senescence requires AMPKα2. *WT* and *Ampka2*$^{-/-}$ MEFs were infected with control or HRAS^{G12V}-expressing retroviruses, and cell proliferation (left panel) and senescence (SA-β-Gal staining, right panel) were analyzed. n=3 experiments for growth curves (assayed in triplicate), n=2 for SA-β-Gal assays; error bars represent S.E.M. Statistical differences were determined by Student's t test; *p<0.05. **(c)** C/EBPβ DNA binding is not affected by loss of

AMPKα1. AMPKα1 was depleted in *WT* MEFs by shRNA knockdown, without or with expression of $HRAS^{G12V}$. Nuclear extracts were analyzed by EMSA using a canonical C/EBP site probe. **(d)** RAS-induced activation of C/EBPβ DNA binding is disrupted in *Ampka2*$^{-/-}$ MEFs. Nuclear extracts were analyzed by EMSA using a canonical C/EBP site probe. Levels of C/EBPβ, p-ERK and total ERK are also shown. **(e)** Analysis of SASP gene expression in *WT* and *Ampka2*$^{-/-}$ MEFs by qRT-PCR. n=2 biological replicates, each sample assayed in triplicate. Values are averages and error bars represent S.D. Statistical significance was calculated using Student's two-tailed t test; *$p<0.05$.

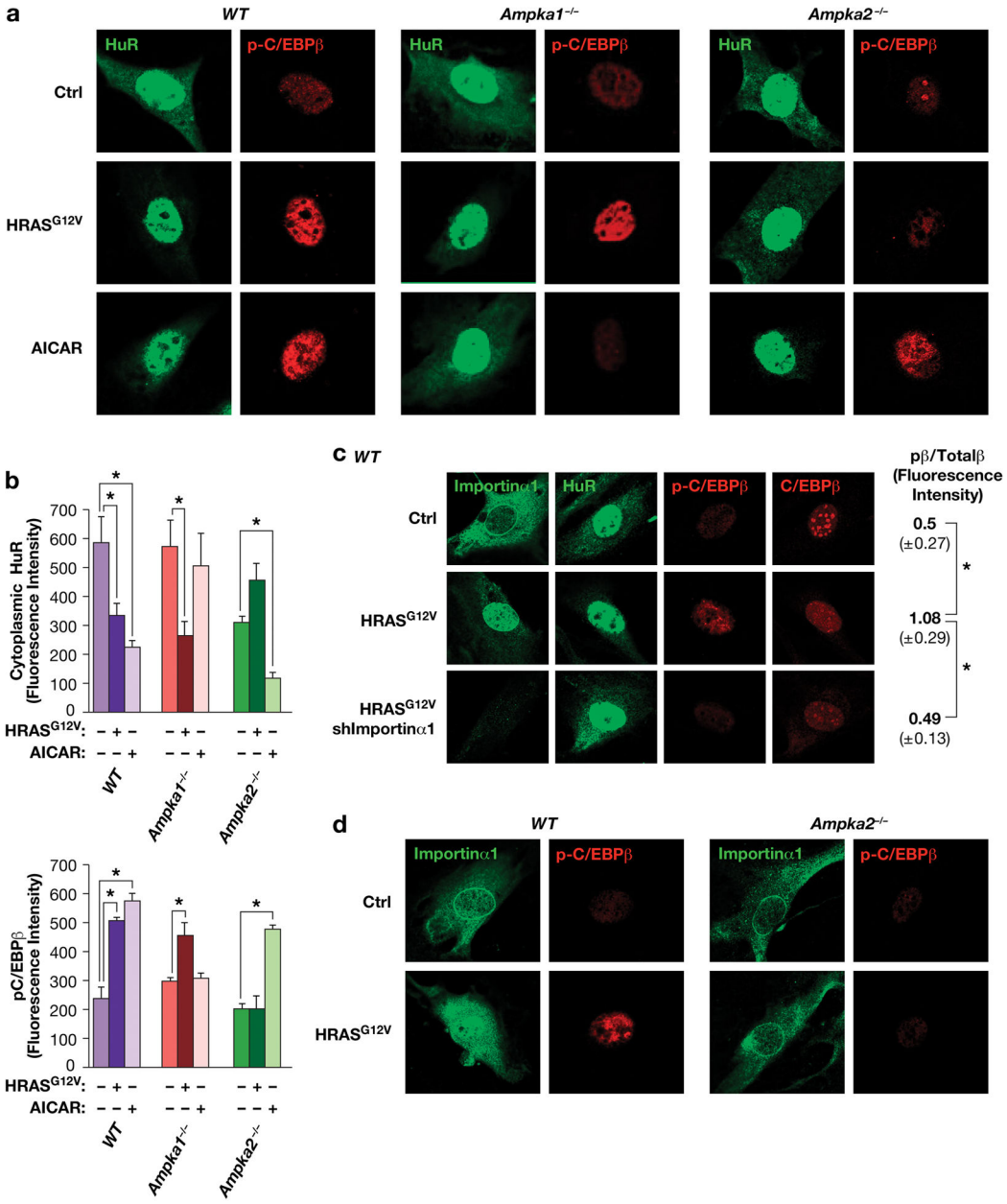

Figure 5.

AMPKα2 is required for HuR translocation and C/EBPβ phosphorylation induced by HRAS^{G12V} but not AICAR. **(a)** Control, HRAS^{G12V}-expressing and AICAR-treated MEFs (*WT*, *Ampka1*$^{-/-}$ and *Ampka2*$^{-/-}$) were analyzed by IF staining to assess HuR localization and p-C/EBPβ (Thr188) levels. **(b)** Cytoplasmic HuR levels and p-C/EBPβ:total C/EBPβ ratios were determined by quantitating images from the experiment of panel **(a)**. n=4 cells; error bars represent S.E.M. Statistical differences were determined by Student's t test; *p<0.05. **(c)** The nuclear transport chaperone, Importin α1, undergoes HRAS^{G12V}-induced nuclear translocation and is required for HuR shuttling and C/EBPβ activation. *WT* MEFs were infected with control or HRAS^{G12V}-expressing retroviruses, without or with Importin

α1 knockdown (shImportin α1). Cells were immunostained for Importin α1, HuR, p-C/EBPβ, and total C/EBPβ. p-C/EBPβ:total C/EBPβ ratios are shown at the right. n=4 cells; error bars represent S.E.M. Statistical differences were determined by Student's t test; *p<0.05. **(d)** AMPKα2 is required for nuclear translocation of Importin α1. *WT* and *Ampka2*$^{-/-}$ MEFs were analyzed for HRAS^{G12V}-induced Importin α1 nuclear re-localization and C/EBPβ phosphorylation (Thr188).

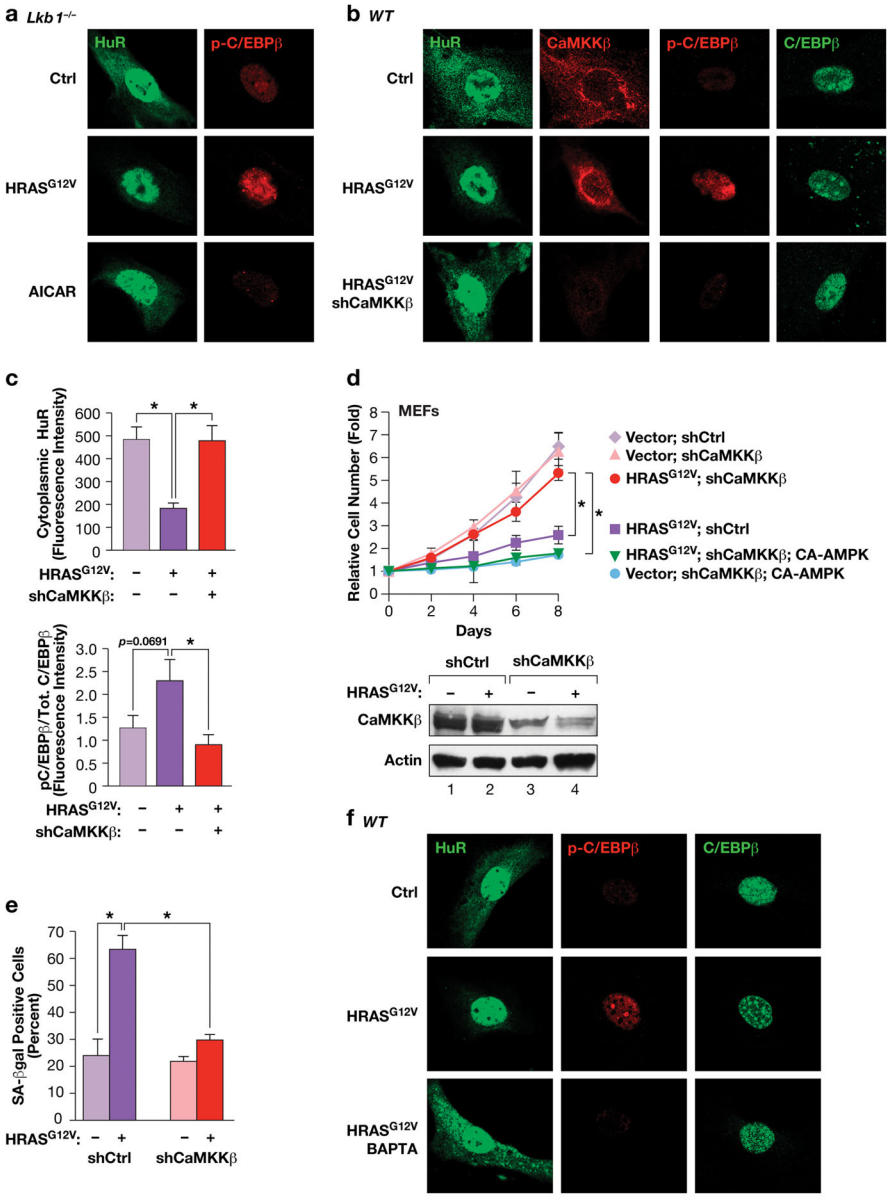

Figure 6.

The AMPK kinase CaMKKβ, but not LKB1, controls HRAS^{G12V}-induced nuclear translocation of HuR and C/EBPβ activation through a Ca^{++}-dependent pathway. **(a)** IF staining of HuR and p-C/EBPβ in control and HRAS^{G12V}-expressing or AICAR-treated *Lkb1*$^{-/-}$ MEFs. **(b)** CaMKKβ depletion prevents HRAS^{G12V}-induced activation of the HuR-C/EBPβ pathway. *WT* MEFs expressing non-specific or shCaMKKβ hairpin RNAs, ± HRAS^{G12V}, were analyzed by IF staining for HuR, CaMKKβ, p-C/EBPβ (Thr188) and total C/EBPβ. **(c)** Quantification of cytoplasmic HuR and p-C/EBPβ:total C/EBPβ ratios from the experiment of panel **(b)**. n=7 cells; error bars represent S.E.M. Statistical differences were determined by Student's t test; *p<0.05. **(d)** Proliferation assays were performed using the cells described in panel **(b)** without or with expression of CA-AMPKα2. n=3; error bars represent S.E.M. Statistical differences at day 8 were determined by Student's t test;

*p<0.05. Lower panel: immunoblot confirming CaMKKβ depletion. **(e)** Effect of CaMKKβ depletion on RAS-induced senescence (SA-β-Gal positive cells). n=130 cells scored from two independent experiments; error bars represent S.E.M. Statistical differences were determined by Student's t test; *p<0.05. **(f)** The Ca^{++} chelator, BAPTA, blocks $HRAS^{G12V}$-induced HuR nuclear translocation and C/EBPβ phosphorylation. Control and $HRAS^{G12V}$-expressing MEFs were treated with vehicle or 10 μM BAPTA for 2 hr prior to fixation. The cells were immunostained for the indicated proteins.

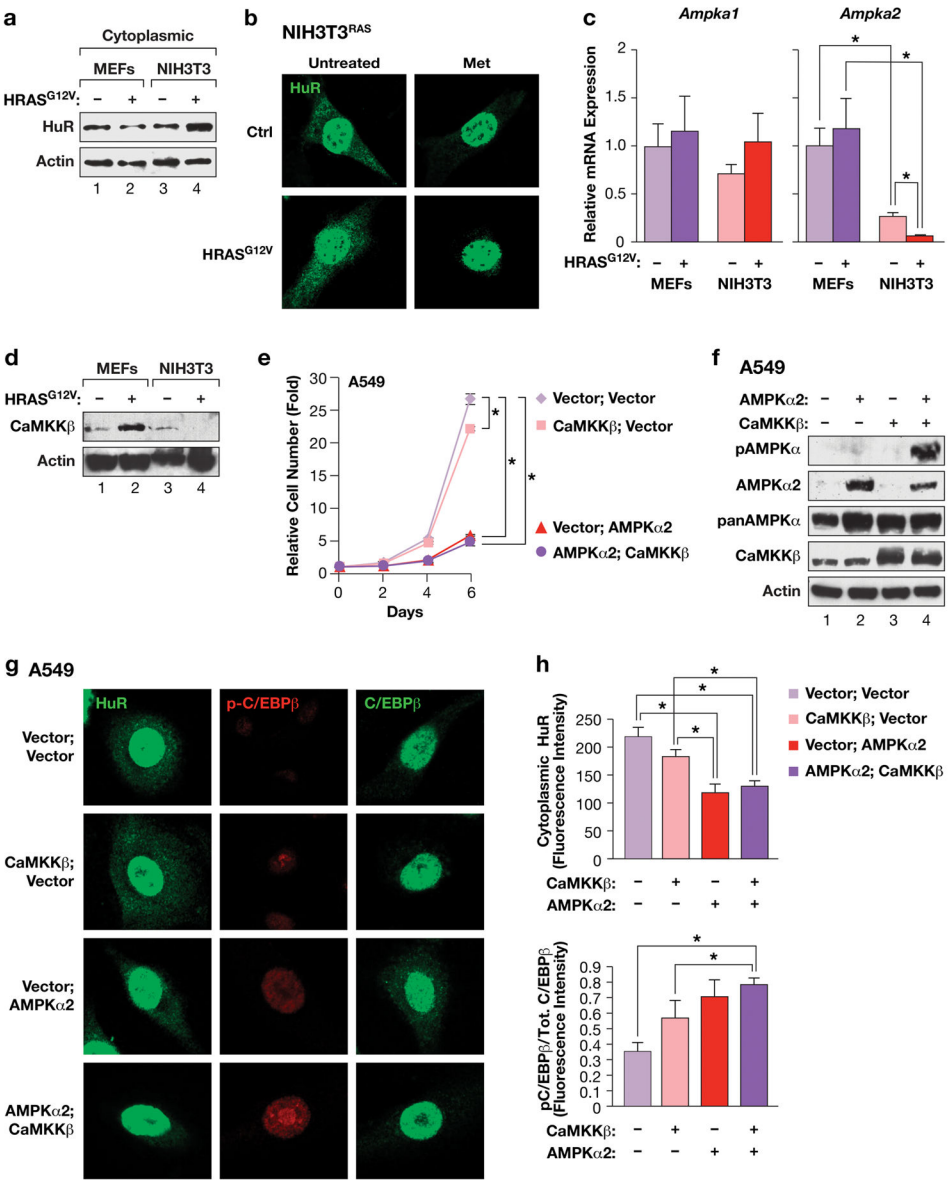

Figure 7.

Proliferation of RAS-transformed cells is associated with elevated cytoplasmic HuR and requires down-regulation of AMPKα2 and CaMKKβ. **(a)** Immunoblot of cytoplasmic HuR levels in MEFs and NIH3T3 cells, without or with expression of $HRAS^{G12V}$. **(b)** Immunostaining of HuR in control or $HRAS^{G12V}$-transformed NIH3T3 cells, ± metformin treatment. **(c)** *Ampka1* and *Ampka2* mRNA levels in MEFs and NIH3T3 cells, ± $HRAS^{G12V}$. Transcript levels were determined by qRT-PCR. n=3 independent biological replicates, each sample assayed in triplicate; error bars represent S.D. Statistics were calculated using Student's two tailed t test.; *p<0.05. **(d)** Immunoblot comparing CaMKKβ levels in MEFs and NIH3T3 cells, without or with expression of $HRAS^{G12V}$. **(e)** Proliferation of A549 cells over-expressing AMPKα2 and/or CaMKKβ. n=2 independent biological replicates, each time point assayed in triplicate; error bars represent S.E.M.

Statistics were determined for day 6 using Student's two tailed t test.; *p<0.05. **(f)** Immunoblot showing over-expression of AMPKα2 and CaMKKβ and CaMKKβ-dependent phosphorylation of AMPKα2 in A549 cells. Lysates from the cell populations described in panel **(e)** were analyzed on blots probed with the indicated antibodies. The anti-p-Thr172 (AMPKα) antibody recognizes modified forms of both AMPKα isoforms. **(g)** IF imaging of A549 cells expressing AMPKα2 and/or CaMKKβ. Cells were immunostained for HuR, or p-C/EBPβ and total C/EBPβ. **(h)** Quantitation of cytoplasmic HuR levels and p-C/EBPβ:total C/EBPβ ratios in the cells described in panel **g**. n=9 cells; error bars represent S.E.M. Statistical differences were determined by Student's t test; *p<0.05.

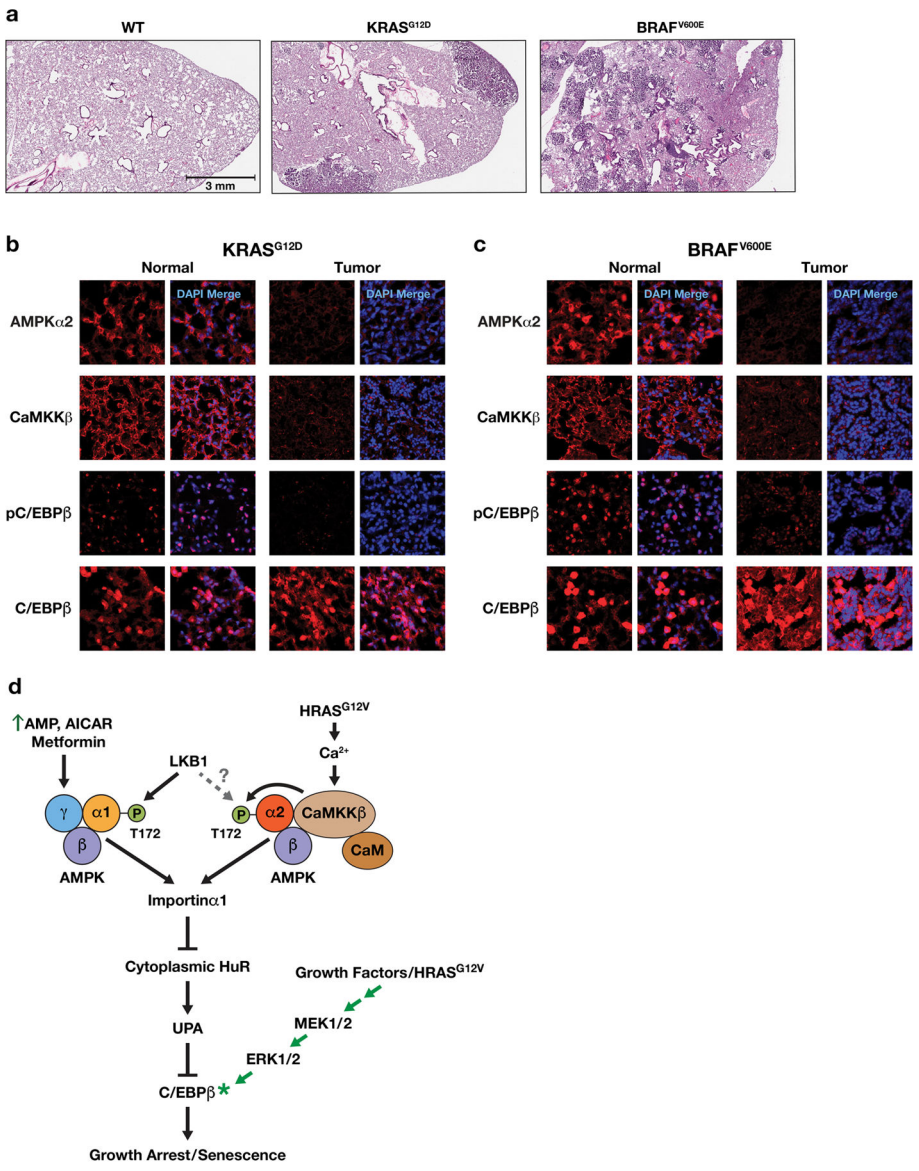

Figure 8.

AMPKα2, CaMKKβ and p-C/EBPβ levels are markedly decreased in *KRAS*^{G12D}- and *BRAF*^{V600E}-driven mouse lung tumors. **(a)** H&E stained lung areas from a normal *WT* mouse, a *Kras*$^{LA2/+}$ mouse[45] containing adenocarcinomas (ADC) and a *LSL-BRAF*^{V600E}/+ animal[46] bearing multiple adenomas. **(b)** Normal and lung tumor areas from a 165 day-old *Kras*$^{LA2/+}$ mouse; sections were immunostained for AMPKα2, CaMKKβ, p-C/EBPβ (Thr188) and total C/EBPβ. **(c)** Normal and lung tumor areas from a 190 day-old *LSL-BRAF*^{V600E}/+ animal (103 days after intratracheal instillation of Ad.Cre virus); sections were immunostained for AMPKα2, CaMKKβ, p-C/EBPβ (Thr188) and total C/EBPβ. **(d)** Model depicting AMPK-dependent pathways that mediate C/EBPβ activation and senescence in response to energy stress/AMPK agonists or oncogenic RAS. AMPK signaling suppresses the UPA mechanism that inhibits C/EBPβ activation and thus licenses

C/EBPβ activation. To become activated, C/EBPβ also requires signaling through the RAS-ERK cascade to induce phosphorylation on Thr188 as well as other modifications[5,62].